

Final Report

A Next-generation Model of Juvenile Salmon Migration Through the Sacramento-San Joaquin Delta

Project co-PIs:

Peter Raimondi (UC Santa Cruz)
Andrew Hein (NOAA NMFS, UC Santa Cruz)
Vamsi Sridharan (UC Santa Cruz)
Eric Danner (NOAA NMFS)
Steven Lindley (NOAA NMFS)

TABLE OF CONTENTS

EXECUTIVE SUMMARY.....	ES-1
ACKNOWLEDGEMENTS.....	AK-1
1. STUDY DESCRIPTION.....	1
1. Study objectives and modeling goals.....	1
2. DATA SOURCES AND DATA PROCESSING.....	1
3. DATA ANALYSES AND RESULTS.....	2
1. Juvenile salmonid movement behavior relative to fine-scale flows.....	2
2. Hydrodynamic flows and migration patterns through Delta reaches.....	3
3. Interactions with predators.....	3
4. Population-scale movement patterns.....	4
5. Data Analysis Conclusions and Relevance for <i>ePTM v2</i> Design.....	5
4. <i>ePTM VERSION 2: MODEL DESIGN AND IMPLEMENTATION</i>.....	5
1. Salient processes represented in the model and empirical justification.....	5
2. Within-channel movements: locomotion and model hydrodynamics.....	5
3. Routing at channel junctions.....	6
4. Predation mortality and survival.....	6
5. <i>ePTM VERSION 2: MODEL CALIBRATION AND EVALUATION</i>.....	6
1. Model calibration.....	6
2. Out-of-sample model evaluation	7
6. REPORTING REQUIREMENTS AND DISCUSSION.....	7
1. Results and conclusions of project hypotheses.....	8
2. Discussion of objectives and whether and how they were met.....	8
3. Discussion of unmet objectives and future alternative approaches.....	9
4. Data and code delivery and management.....	9
5. How project addressed Water Quality, Supply and Infrastructure Improvement Act of 2014, and the California Water Action Plan.....	10
6. Conclusions.....	10
7. REFERENCES.....	R1

FIGURES.....	F1
---------------------	-----------

APPENDICES

APPENDIX A: STRUCTURE, FORMULATION, CALIBRATION, AND EVALUATION OF THE ENHANCED PARTICLE TRACKING MODEL VERSION 2 (<i>ePTM v2</i>).....	i
APPENDIX B: CHANNEL CURVATURE.....	xix
APPENDIX C: FLOW PROFILES	xx
APPENDIX D: MODEL TUNING	xii
APPENDIX E: ROUTING AT COMPLEX JUNCTIONS.....	xxii
APPENDIX F: PARAMETER ANALYSIS AND SCREENING.....	xxvi
APPENDIX G: INITIAL PARAMETER SELECTION.....	xxvii
APPENDIX H: GOODNESS-OF-FIT MEASURES.....	xxviii
APPENDIX I: SURVIVALS AT CHIPPS ISLAND.....	xxix

EXECUTIVE SUMMARY

While migrating through the Delta and its tributaries, Chinook salmon and steelhead move through diverse habitats, encounter predators, interact with dynamic flows, and are impacted by human-made structures and altered hydrology. There is scientific consensus and agreement among policy makers that integrated system-level models and ecosystem-level management are needed to effectively manage salmonid populations and other key natural resources in the California Central Valley. An essential requirement for species monitoring and management is that models are able to efficiently assimilate new data, and that they can be used to evaluate in-season scenarios as well as future scenarios quickly and robustly. It is also important that the physical and biological processes represented in such models be based upon empirical data from studies of fish survival and behavior conducted in the Delta. Better fundamental understanding of how salmonids migrate through the Sacramento-San Joaquin Delta and the incorporation of this knowledge into a decision support model will help more optimally manage water to meet the Water Action Plan target of achieving co-equal goals for the Delta.

The objective of the present study was to meet these demands by integrating, analyzing, and assimilating data from a wide range of studies of out-migrating salmonids in the Delta to produce a data-driven modeling framework capable of predicting salmonid movements and survival through the system. Analyses focused on data sources from acoustic telemetry studies at both large extent/coarse spatial resolution (large-scale acoustic telemetry networks), and local extent/fine spatial resolution (two-dimensional hydrophone arrays at Delta junctions). These data were combined with bathymetric data and hydrologic data and modeling to study fish movements and interactions with predators in the dynamic flows within the Delta. Our results led to a data-informed set of behavioral rules that characterize how fish move through the system, and how they interact with predators.

To translate the behavioral and physical processes observed in data into predicted migration and survival patterns, and to provide a decision support tool for water management seeking to meet co-equal goals, we developed a computational, agent-based simulation model called the enhanced particle tracking model version 2, or *ePTM v2*. We present the motivating data behind the model and describe the model's structure. We then show that, by fitting model parameters through a calibration procedure, the model is capable of reproducing survival and movement patterns of late fall run Chinook migrations through the Delta. Finally, we demonstrate that the model can also be used in forecast mode, to make predictions about new data on which it was not trained. We illustrate this by using the model to forecast through-Delta survival and routing of fall and winter run Chinook released from 2012 through 2017 in the Sacramento River. The model produces accurate predictions of survival and routing of these releases across a ten-fold range of flows in the Sacramento River. This indicates that the model can make accurate out-of-sample predictions, and that it can do so across the broad range of hydrologic conditions experienced during very different water years.

We conclude by discussing how the specific study objectives were addressed, and how the work as a whole addresses goals laid out in the Water Quality, Supply and Infrastructure Improvement Act of 2014 (Proposition 1), and the 2016 California Water Action Plan

ACKNOWLEDGEMENTS

The project team would like to acknowledge the following people (listed in alphabetical order) for their help in providing, interpreting, and processing data from acoustic telemetry and hydrologic studies conducted within the Delta:

Arnold Amman, National Marine Fisheries Service, National Oceanic and Atmospheric Administration

Rebecca Buchanan, Columbia Basin Research, School of Aquatic and Fishery Sciences, University of Washington, Seattle, WA

Jon Burau, California Water Science Center, United States Geological Survey

Josh Israel, United States Bureau of Reclamation

Doug Jackson, QEDA Consulting LLC.

Sam Johnston, HTI Sonar

Kate Le, California Department of Water Resources

Jacob McQuirk, California Department of Water Resources

Cyril Michel, Institute of Marine Sciences, University of California Santa Cruz

Jeremy Notch, Institute of Marine Sciences, University of California Santa Cruz

Russel Perry, Western Fisheries Research Center, United States Geological Survey

Adam Pope, Western Fisheries Research Center, United States Geological Survey

1. STUDY DESCRIPTION

Protecting native species and ecosystems is a primary goal of management and conservation efforts in the Sacramento-San Joaquin Delta (DSC 2013; NMFS 2014; CDFW 2018; DSC 2019; DSC 2021a; DSC 2021b). Facilitating successful migrations of threatened, endangered, and economically important migratory fishes such as Chinook salmon and steelhead is an integral but challenging element of this goal. Every year, juvenile Chinook salmon and steelhead (hereafter referred to as salmonids) migrate to the Pacific Ocean, passing through the Delta in the process (MacFarlane and Norton 2002; Chapman *et al.* 2013). Studies of survival of juvenile salmonids through the Delta have shown that mortality of these species can be extremely high (e.g., Perry *et al.* 2010; Perry *et al.* 2013; Perry *et al.* 2018; Buchanan *et al.* 2020; Michel *et al.* 2020). As a result, management and restoration efforts have taken on the objective of improving salmonid migration success through the Delta (e.g., CNRA 2017b, 2016 California Water Action Plan). However, designing management and restoration plans that maximize salmonid migration success requires quantitative models that can project the impact of proposed actions on migration success at the scale of the entire Delta. Such models are crucial not only for near-term planning, but also for designing management strategies that are resilient under climate change.

The objective of this study was to build a model of salmonid migration through the Delta to enable impacts of system hydrology, ecosystem processes, and management actions on salmonid migration and survival to be assessed quantitatively. Over the past decade, research groups working in the Delta, including teams from UC Santa Cruz and NOAA, have collected rich datasets related to salmonid survival and migration that span the range of scales relevant to migration outcomes (e.g., DWR 2012; SJRGA 2013; AECOM *et al.* 2015; DWR 2015; DWR 2016; Demetras *et al.* 2016; Perry *et al.* 2018; Michel *et al.* 2020; Notch *et al.* 2021). A central element of the present study was to integrate relevant information from these diverse data sources to inform development of our modeling framework.

1.1 Study objectives and modeling goals

The overarching objective of this project was to integrate and analyze existing data collected at several distinct spatial scales to identify the salient processes that influence movement and survival of out-migrating juvenile salmonids in the Delta. We then sought to build a model of salmon out-migration that captured these salient processes, while retaining speed and interpretability. We also wished to evaluate model predictions across a range of flow conditions. Specific objectives to accomplish these goals were:

1. Analyze data from studies of salmonid migration in the Delta to identify salient processes impacting movement and mortality through the system.
2. Use these data to design a simulation model of salmonid migration through the Delta, including navigation and predation modules based on how migrants are affected by predators, flows, and other environmental variables.
3. Achieve a desirable balance between model speed and robustness to diverse and changing environmental conditions.
4. Improve hydrodynamics module by improving terms used for physical drivers of migration dynamics in the model.
5. Evaluate and validate the model's ability to robustly predict salmonid movements and fates across environmental conditions.

2. DATA SOURCES AND DATA PROCESSING

The focus of our analyses was to reveal how out-migrating salmonids navigate the Delta and either perish or survive. We, therefore focused on a subset of data from past studies most likely to provide information on these processes. Data sources fell into two categories: studies of salmonid movements using large-

scale acoustic receiver arrays, and studies of fine-scale movements of fish through channels and in the vicinity of junctions. We also used hydrodynamic and bathymetric data.

Large-scale acoustic receiver arrays and tagging data. The first class of data used in analyses came from large-scale acoustic telemetry studies. Data in this class included data from large-scale late-fall run Chinook acoustic telemetry studies conducted from 2006-2010 in the Sacramento River and Delta (Perry *et al.* 2010; Perry *et al.* 2012; Perry *et al.* 2018), and acoustic telemetry studies of fall and winter run Chinook releases conducted from 2012-2017 as part of the California Enhanced Acoustic Tagging Project (<https://oceanview.pfeg.noaa.gov/CalFishTrack/>). A second data source in this class included three years of data (2011-2013) from a study of steelhead out-migration conducted in the southern portion of the Delta (SJRGA 2013). This dataset was provided to us by Rebecca Buchanan (Univ. Washington) facilitated by Josh Israel (USBR). Raw acoustic telemetry detections had been pre-processed prior to us receiving the data. Data pre-processing steps are described in Buchanan *et al.* (2020).

Fine-scale two-dimensional data at key Delta junctions. The second class of data used in analyses came from fine-scale hydrophone arrays at the Head of Old River (2011-2012, AECOM *et al.* 2015) junction on the San Joaquin River, and Georgiana Slough junction (2012, 2014, DWR 2015; 2016) on the Sacramento River. Data were provided by Sam Johnston (HTI Sonar) facilitated by Jacob McQuirk of California Department of Water Resources. We also used data from tracked predators (2012) collected as part of the Head of Old River study. Prior to analyzing data, we applied a processing pipeline that consisted of breaking tracks from each fish into segments if subsequent locations were separated by more than 30 s in time. Within each segment, we smoothed tracks using a third-order Savitzky–Golay filter with filter length of 22 s. Positions were also interpolated to a regular time interval of 2 seconds.

Hydrologic and bathymetric data. Three sources of hydrologic data were used. The first was fine-scale surface flow data collected using acoustic Doppler current profilers (ADCPs) at the Head of Old River (2012) and Georgiana Slough (2012, 2014) junctions (Stumpner n.d. a; b; c). These ADCP data were collected by USGS in collaboration with AECOM, Ltd. These data were provided to us by Kate Le (DWR). In addition to flow fields, channel bathymetry data were obtained from the 2010 California Department of Water Resources and the US Geological Survey's 2-m-resolution multibeam sonar survey (Wang *et al.*, 2018). Two-dimensional near-surface velocity fields and bathymetry data were used to develop a three-dimensional computational fluid dynamics model of the Head of Old River junction. Two-dimensional near-surface velocity fields at Georgiana Slough were used in analyses of spatial patterns of fish movement. The second source of hydrologic data used in our analyses was channel water gauge data housed at the California Department of Water Resources' California Data Exchange Center (CDEC) database (DWR 2020). A QAQC protocol was applied to gauge data to ensure no erroneous values were included in the analysis (Sridharan 2018). When gauge data were unavailable or deemed unreliable, DWR's DSM2 hydrodynamic model was used to simulate flows (DWR 1998).

3. DATA ANALYSIS AND RESULTS

As outlined above, one of the primary motivations for the work described in this report was to link process-based modeling of salmonid migration and survival much more tightly with data from studies of out-migrating juvenile salmonids in the Delta. Our objective in the data analysis portion of this project was to extract as much information as possible from acoustic tracking datasets by combining datasets collected at several different spatial scales, and pairing them with hydrologic data and modeling. By doing this, we acquired key pieces of information that helped define the structure of the computational model of salmonid out-migration developed in Section 4.

3.1 Juvenile salmonid movement behavior relative to fine-scale flows

To determine how juvenile Chinook salmon move in relation to local flow patterns, we first conducted a detailed analysis of two-dimensional fish tracks collected from the Head of Old River junction on the San Joaquin River (AECOM *et al.* 2015). We chose this data set due to the tractable

domain size, which made it suitable for computational fluid dynamic (CFD) modeling, and the availability of both two-dimensional flow measurements and fine scale juvenile Chinook salmon tracking data. The results of our analyses of flows, salmon movements, and trajectory forecasting are described in the published manuscript Olivetti *et al.* (2021), included with this report. The results most relevant to the migration model development in Section 4 are as follows.

Swimming and orientation relative to flows. Juvenile Chinook salmon regularly orient their swimming velocities in ways that are not aligned with local flow (Olivetti *et al.* 2021). This results in oceanward ground speeds that are significantly slower than that of the mean flow. However, the degree to which fish direct locomotion against flows changes as flow conditions change.

Locomotion force production meets or exceeds force imposed by flow. The forces produced by juvenile Chinook often meet or exceed the dragging force imposed on them by the water. From a model design perspective, this suggests (1) that fish are capable of swimming with flows, holding position in flow, and swimming upstream against flows, and (2) that both hydrodynamics and swimming behavior are likely to be required to accurately model movements of fish through the system.

Consistency of fish swimming behaviors across individual migrants. Migration behavior of different individual fish in a population can be accurately predicted using the same behavioral rules (Olivetti *et al.* 2021). We showed that movement trajectories could be predicted using a behavioral rule set embodied in a recurrent neural network model, moreover this rule set can be used to forecast fish movements in out-of-sample data. This suggests that different individuals use navigation rules that are similar enough to be described accurately by the same quantitative rule set.

3.2 Hydrodynamic flows and migration patterns through Delta reaches

Fine-scale movements of steelhead and Chinook in the north Delta. Consistent with findings of Olivetti *et al.* (2021), we found that both juvenile Chinook and steelhead in the vicinity of the Georgiana Slough junction on the Sacramento River swim both with and against local flows (Fig. 3.2.1A-B left, means both above and below 1:1 line); on average, oceanward ground velocity of fish is positively correlated with oceanward flow velocity and strongly positively correlated with oceanward swimming velocity. We also found that fish swimming velocities show strong signs of temporal autocorrelation (Fig. 3.2.1C). Finally, during tidal conditions in which flow is reversed (i.e., oceanward flow is negative), swimming velocities are primarily directed oceanward (Fig. 3.2.1D), and the speed of oceanward swimming increases with increasing landward tidal flow (Fig. 3.2.1E). This suggests fish can maintain position and even advance oceanward against incoming tidal flows.

Movements relative to flow throughout the Delta. Figure 3.2.2 shows the mean migration rate of experimental release of steelhead, fall, late fall, and winter run Chinook salmon. The figure reveals several patterns. Firstly, the rate of migration of both species and all runs studied show a consistent pattern as flow transitions from primarily riverine (Fig. 3.2.2A left side of plot) to primarily tidal (Fig. 3.2.2A, right side of plot). In particular, migration rate of fish relative to mean flow shifts from being negative, indicating that fish migrate more slowly than the mean flow, to positive, indicating that fish migrate more rapidly than mean flow. The second pattern evident in this analysis is that the dispersion of fish, measured as the standard deviation of travel times through a reach, increases from less tidal to more tidal regions of the system (Fig. 3.2.2.B), but in all regions, far exceeds hydrodynamic dispersion alone. This again suggests, consistent with results of Olivetti *et al.* 2021 and Fig. 3.2.1, that swimming behavior can exhibit a dominant effect on movement rates.

Movements under strongly tidal conditions. Figure 3.2.3 shows arrival patterns at hydrophone detection stations in the strongly tidal portion of the system. This plot shows the total number of arrivals by tidal phase. Numbers indicate total arrival events. The month ranges on top indicate the months during which the fish entered the Delta. Again, we see significantly more number of fish arriving during ebb tides than during flood tides at telemetry stations irrespective of species or run.

3.3 Interactions with predators

Another key process influencing migration outcomes in Delta reaches is interactions with predators. Many analyses of acoustic telemetry data from the Sacramento and San Joaquin Rivers as well as the Delta have estimated salmonid survival (or, equivalently, mortality) (Perry *et al.* 2018; Hance *et al.* 2021; Michel *et al.* 2020; Michel *et al.* 2021; Notch *et al.* 2020). These past findings provided a basis from which to formulate the predation module of *ePTM v2*; however, because the proposed framework for our model involved spatially-explicit movements of simulated migrant through the system (see Section 4 below), we wished to test assumptions about the processes by which salmonids interact with predators in space to identify an optimal model design.

To estimate spatial patterns of exposure of juvenile Chinook salmon to predation risk, we analyzed the two-dimensional tracking dataset collected Head of Old River in 2012. We combined this data set with relocation data for four species of predators tagged and detected over the same period of time as Chinook: striped bass ($n = 19$), largemouth bass ($n = 13$), channel catfish ($n = 6$), and white catfish ($n = 1$; AECOM 2015). To determine whether predator occupancy was concentrated in particular subregions of the domain, we subdivided the region into spatial bins of ~ 12.5 square meters, summed relocations in each of these bins, and divided by sampling days to compute a predator relocation density metric in units of predator relocations per meter squared per day. To create a smoothed estimate of this density metric across the Head of Old River domain, we fitted a generalized additive model to predator data, which included main effects of depth, distance from shore, and sun (i.e., day vs. night), and all two-way interactions between these variables. Using this fitted model, we generated predictions for mean predator density across the domain (Figure 3.3.1A). To understand how the spatial landscape of predators translates to salmonid exposure to predators during migration, we computed the predator density along each observed Chinook path. We summed this measure across time for each track to produce an integrated measure of predation risk we refer to as predator exposure. For reference, we recomputed this measure for a null model in which random walkers traverse the domain. The lengths of random walks were chosen to match those of observed salmon tracks. Figure 3.3.1B compares predator exposure values of observed salmon tracks to the random walk model. The comparison suggests that, when integrated over the diel cycle and averaged over the population studied here, migrating chinook experience similar predator exposure to that expected under an unbiased random walk. Finally, to determine whether exposure depended on the length of a given trajectory through the region, we computed exposure as a function of track length (Fig. 3.3.1C), which indicated a positive correlation. This suggests that longer, more tortuous tracks through the domain lead to a higher predator exposure than do shorter, more direct tracks. This analysis supports our formulation of the predation module in *ePTM v2* (see Section 4 below).

3.4 Population-scale movements patterns

Many animal migration models rely on two key assumptions: that populations of migrants can be represented by simulating populations of virtual migrants in which (1) all simulated individuals follow the same behavioral rules, and (2) interactions among individuals are weak enough that a reasonable approximation of migration behavior can be achieved by simulating many non-interacting individuals (but see Berdahl *et al.* 2016). If these assumptions are reasonable and the behaviors of individuals are either constant, or at least statistically stationary in a given region over time, it should be possible to represent movements of a migratory population using either Lagrangian simulations or a continuum formulation, where the population is modeled as a density (or distribution) of individuals distributed over space. An example of the latter formulation is an advection-dispersion (or advection-dispersion-mortality) model that tracks the time-evolution of the spatial distribution of migrants as they move through the system. In Sridharan and Hein (2019) we applied a one-dimensional Advection-Dispersion (AD) model to see if such a model could recover movements of acoustically tagged steelhead in the San Joaquin River. Figure 3.4.1 shows results of that analysis, which indicated strong agreement between predicted and observed arrival rates of steelhead at hydrophone arrays. Further analyses of steelhead movements through the Delta (not included here) confirmed that population movement patterns across the Delta can be well described by advection-dispersion-mortality models with spatially varying parameters. Thus, despite the complex hydrology of the Delta and biological variation among individual migrants, models that

represent the spatial distribution of fish as they move directionally and disperse from one another can accurately capture key features of population movement patterns. The *ePTM v2* model developed in Section 4 has a very different structure from these simple continuum models, but it too depicts migrants as populations of non-interacting individuals that use the same migration rules.

3.5 Data Analysis Conclusions and Relevance for ePTM Design

The analyses in the preceding sections provide the empirical support needed to motivate the structure and parameterization of the Next Generation ePTM model. The most essential elements of these findings are summarized in this section.

Navigation and movements relative to flows. Analyses of both two-dimensional datasets and large-scale telemetry network data provide important insights about the rules by which juvenile salmonids move relative to flows. The first of these is that, under weakly tidal conditions, juvenile salmonids frequently direct locomotion against prevailing flows (Olivetti et al. 2021; Fig. 3.2.1). They also display temporally autocorrelated movements (Fig. 3.2.1). Larger-scale patterns of migration rate relative to flow indicate a shift from travel speeds that are slower than mean flow, to speeds that exceed mean flow as fish move from more riverine to more tidal conditions (Fig. 3.2.2). In reversing tidal regions, there is strong evidence for differential oceanward movements during ebb tides (Fig. 3.2.3) for both steelhead and Chinook salmon, likely driven by swimming/holding against incoming tidal flows (Fig. 3.2.1).

Interactions with predators. Past analyses suggest that predation mortality is important in the Delta, and varies in space (Demetras et al. 2016, Michel et al. 2020). Our analysis adds to past information by resolving tracks of freely-swimming fish as they move through regions of variable predator density. Our findings suggests that (1) diel-averaged exposure of salmonids to spatially distributed predator hotspots is reasonably well approximated by a random walk through the region, and (2) exposure depends not only on time spent in the region (Michel et al. 2020) but also distance traveled within a reach (Figure 3.4.1C).

4. ENHANCED PARTICLE TRACKING MODEL VERSION 2 (ePTM v2): MODEL DESIGN AND IMPLEMENTATION

The *ePTM v2* is a coupled physical-biological Lagrangian particle tracking model that simulates the movements and mortality of juvenile salmonids in the Delta. We based *eTPM v2* on DSM2's particle tracking model (PTM; DWR 1998), but *ePTM v2* uses different numerical methods and, most importantly, it incorporates data-driven models of salmonid behavior during migration. Full details of the model structure and parameterization are given in Appendix A but the basic elements of the model are described in this section.

4.1 Model structure

Based on our analyses, the structure of *ePTM v2* is designed to simulate three key processes related to salmonid migration through the Delta (Figure 4.1.1): within channel movements, routing at channel junctions, and mortality. At each simulation timestep, simulated migrants move through the channel where they are located, experience a probability of mortality, and, if they are in the vicinity of a channel junction, move into one downstream channel or the other. By iterating this process over many timesteps, *ePTM v2* predicts how populations of migrants move through the Delta, and when and where mortality occurs. The following sections describe how the model simulates these processes.

4.2 Within-channel movements: locomotion and model hydrodynamics

Swimming locomotion in *ePTM v2* involves a sequence of behavioral “choices” each migrant makes at each simulation timestep. These should be interpreted as temporally coarsened representations of the fine scale swimming behaviors (Appendix A) exhibited by migrants, which can vary in space, time,

and among individual migrants (Olivetti *et al.* 2021, Section 3). The model represents these behaviors as a hierarchy of stochastic decisions. At each simulation timestep, the sequence of behavioral choices involves the following: (1) hold or swim; *if swim* (2) select swimming direction *and* (3) select swimming speed. The outcome of these behavioral decisions at each timestep are stochastic, and they are produced by a set of behavioral functions that provide the probabilities of each action based on the physical conditions and location of the animal. The forms of functions are selected based on empirical evidence from our analyses of salmonid migration behavior in the Delta (Section 3), acknowledging that some simplifying assumptions are necessary to ensure that parameters are statistically identifiable and that computation times during model runs are kept within an acceptable range. The decision to hold or swim depends on the migrant’s location in the system and the flow it experiences. Swimming direction is influenced by the migrant’s previous swimming direction, as well as the flow it experiences. Swimming speed is drawn from an empirically constrained distribution of swimming speeds (see Appendix A).

4.3 Routing at channel junctions

A second important process that determines how salmonids move through the Delta is how animals move into one downstream channel or another at junctions. Sridharan *et al.* (2017) demonstrated the importance of correctly representing the movement of simulated fish through channel junctions. In *ePTM v2*, we allow fish to move into downstream channels at junctions depending on their lateral position relative to the critical streakline (Perry *et al.* 2014), also known as the bifurcating streamline (Sridharan *et al.* 2017; Appendix A).

4.4 Predation and mortality

Based on the analyses in Section 3.4 and past studies (e.g., Demetras *et al.* 2016, Michel *et al.* 2020), we model mortality of out-migrating salmonids as a function of both the time spent in a given region, and the distance traversed during this time span. Our implementation of these processes is based on a modified version of the “*X-T* model” developed by Anderson *et al.* (2005). Mortality is treated as a first order rate process in which the probability of surviving through a given reach decreases with increasing travel time and migration distance. At each simulation time step, simulated fish are assigned a probability of survival that depends on the properties of the reach they are traveling through, the length of the time step, and the distance traveled during that time step (Appendix A). Simulated migrants survive or die depending on this probability.

5. ENHANCED PARTICLE TRACKING MODEL VERSION 2 (*ePTM v2*): MODEL CALIBRATION AND EVALUATION

A detailed account of *ePTM v2* calibration and evaluation is given in Appendix A. In brief, results of the *ePTM v2*, show strong agreement with the major patterns evident in Chinook acoustic telemetry data. Moreover, parameter estimates reflect the behavioral patterns evident in our analyses of empirical data (Section 3). These agreements between model and data suggest that (1) *ePTM v2* is capable of capturing the salient features of salmonid migration through the Delta to make accurate predictions, and (2) the module structure, assumptions, and interpretation of parameters are consistent with empirically observed behaviors of out-migrating fish in the system.

5.1 Calibration: survival patterns

Reach-dependent survival estimates for Delta reaches (Fig. 5.1.1) are illustrated in Figure 5.1.2, which shows the difference between estimated survival computed using Cormack-Jolly-Seber (CJS) analysis of acoustic telemetry data (Perry *et al.* 2010; Perry *et al.* 2018), and survival predicted by *ePTM v2* on the training data. Predicted survival shows strong agreement with data in reaches spanning the Delta. In general, predicted survival estimates are within ± 0.2 of observed survivals throughout the Delta,

indicating that the model captures patterns of survival and mortality across the diverse habitats and hydrologic conditions the system comprises.

A second variable predicted by *ePTM v2* is the distribution of migrant travel times in reaches throughout the system. Acoustic telemetry data yields detections at upstream and downstream stations of a given reach and these detections can be used to compute empirical travel times for all fish detected at both stations. *ePTM v2* can generate travel time predictions for the same fish by initializing simulated migrants at the upstream reach at times that are matched to observed arrival times and then simulating movement of migrants until they arrive at the downstream station. Figure 5.1.1.3 shows travel times, represented as the cumulative distribution function of observed (black) or predicted (red) travel times through the reach for different reach by release group combinations. The model predictions show strong agreement with travel time distributions for nearly all release by reach combinations. This confirms that the model is able to simultaneously capture survival and movement dynamics through the Delta.

5.2 Out-of-sample evaluation

To evaluate predictions of the *ePTM v2* using data that were not included in model fitting, we used data from the California Enhanced Acoustic Tagging Project, which provides arrival data and CJS survival estimates for JSATS-tagged Chinook runs and water years (<https://oceanview.pfeg.noaa.gov/CalFishTrack/>). We used data that met several criteria: (1) runs of Chinook studied were fall or winter, (2) the release group size at the release site was greater than 100 fish, and (3) fish were observed at least at the telemetry stations at Sacramento and either at Chipps Island or Benicia. This resulted in 11 run by release group by water year combinations against which to compare predictions. Survival predictions for out-of-sample runs were produced in the same way as the predictions for the training set (see above). Figure 5.2.1, shows observed and predicted through-Delta survival of Chinook salmon as a function of mean flow in the Sacramento River. Model predictions capture the major patterns evident in data. Firstly, through-Delta survival predictions of the model (Fig. 5.2.1 red squares) compare favorably with direct estimates from data (Fig. 5.2.1, black circles). In most cases, the survival prediction is within 0.2 of the observed survival, and in some cases it is much closer. Secondly, the model recovered the shape and scale of the observed relationship between survival and mean river flow through the Sacramento during migration through the Delta (Fig. 5.2.1, lines and confidence intervals). It is worth emphasizing that not only are all data used to compute observed survival out-of-sample (i.e. they were not used in the model calibration), none of the out-of-sample data (fall and winter run Chinook 2012-2017) overlap in time with the data used in model calibration (late fall run Chinook 2006-2010). We therefore believe this comparison provides a strong test of the performance of *ePTM v2* in forecast mode.

Another aspect of out-of-sample validation is model performance in predicting migration routing. To study how the model performs in predicting out-of-sample route use by salmon through the system, we selected those releases of the JSATS program in which fish passages were recorded through two key junctions along the Sacramento River: the Mainstem Sacramento with Sutter and Steamboat Sloughs, and Georgiana Slough. This resulted in a subset of releases from 2014 and 2015. Results are shown in Figure 5.2.2, which shows observed and predicted salmon detected along different possible routes at the two junctions. To further elucidate the fine-temporal scale of the model, we stratified this comparison by phase of the tide, defined at the junction with Sutter and Steamboat Sloughs with respect to the flow reversal in Steamboat slough, and at the junction at Georgiana Slough with respect to the flow reversal in Georgiana Slough. In both years, the model is able to predict the qualitative patterns in the data correctly, and quantitative routing probabilities to $\pm 20\%$ from the observed values. This performance is favorable given that the routing module in *ePTM v2* has no free parameters, nor was routing information used in model calibration. A fish guidance structure was in place in 2014 at the head of Georgiana Slough with an overall passage efficiency of 0.777 (DWR 2016). This was represented in the model as a particle filter.

6. DISCUSSION

The overarching objective of this project was to analyze a range of pre-existing data sets to identify the salient processes that influence movement and survival of out-migrating juvenile salmonids in the Delta, and to build a model of salmon out-migration that captured these salient processes, while retaining speed and interpretability. In the preceding sections, we describe how we carried out these steps, and report our findings. We also describe the modeling framework, *ePTM v2*, we built based on these analyses. Here, we discuss these results in light of project objectives and hypotheses.

6.1 Results and conclusions of project hypotheses

We began the project with a set of hypotheses related to salmonid out-migration behavior and survival through the Delta. Those hypotheses and our conclusions are listed below.

Hypothesis 1. *Out-migrating salmonids movements through the Delta are influenced by both hydrodynamic forcing and active swimming behavior.* The analysis we describe in Olivetti *et al.* (2021) as well as those presented in Section 3.2 confirm that both hydrodynamic forcing on fish and active swimming behavior combine to determine how fish move through channels in the Delta. Another recent study found similar patterns in Chinook salmon movements, which further supports our hypothesis (Gross *et al.* 2021). The finding that locomotion speeds and forces produced by out-migrating fish often exceed those produced by flow alone underpin the importance of including swimming behavior in any viable process model of salmonid migration in the Delta. The details of how fish swim relative to flow shaped design of the *ePTM v2* navigation module.

Hypothesis 2. *Interactions with fish predators are likely to be an important factor impacting juvenile salmonid survival through the Delta.* Predation mortality has long been suspected to be a significant source of mortality for salmonids in the Delta. Several lines of evidence support the idea that predation of smolts by piscivorous fish may be particularly important (e.g., Demetras *et al.* 2016, Michel *et al.* 2020). The analysis in Section 3.3 of freely swimming smolt trajectories and exposure to predator-dense regions of Delta channels adds support to the body of evidence suggesting that encounters with fish predators are likely to be important during out-migration. This analysis helped guide design of the predation module in *ePTM v2*.

Hypothesis 3. *Spatial and temporal patterns of salmonid migratory movements and survival can be accurately captured by a migration model that combines hydrodynamic forcing on fish with data-driven behavioral migration rules assumed to apply to all migrants.* Our analyses confirmed this hypothesis. In particular, the *ePTM v2* model evaluations show strong agreement with survival and travel time estimates from out-migrating Chinook salmon. This agreement holds across Delta reaches (Fig. 5.1.1 and 5.1.2) and different years with distinct hydrologic conditions (Fig. 5.2.1). Our analyses with simpler PDE-based models (Sridharan and Hein 2019) also support this conclusion, as those models too are able to predict population movement patterns.

6.2 Discussion of objectives and whether and how they were met

All primary project objectives were met. These objectives included the following:

Objective 1. *Analyze data from studies of salmonid migration in the Delta to identify salient processes impacting movement and mortality through the system.* Sections 2-3 of this report describe the data sources and analyses used to achieve this goal. Sufficient data were available to investigate nearly all of the key processes suspected to exert major influence salmonid migration (see Section 6.3 below for several minor exceptions). These data were, therefore, sufficient to guide the design of the next-generation enhanced particle tracking model, *ePTM v2*.

Objective 2. *Use these data to design a simulation model of salmonid migration through the Delta, including navigation and predation modules based on how migrants respond to predators, flows and other environmental variables.* Section 4 and Appendix A of this report describe how the simulation model, *ePTM v2*, was designed based on the analyses carried out to meet Objective 1. In particular, navigation and predation modules incorporated results of our analyses as well as results of past research in the Delta to motivate model structure and evaluate underlying assumptions.

Objective 3. Achieve a desirable balance between model speed and robustness to diverse and changing environmental conditions. Section 4 and Appendix A of this report describe how *ePTM v2*'s flexible and modular parameterization allow it to make predictions across ranges of environmental conditions. Section 5 and Appendix A, describe in further detail how we evaluated model robustness across such conditions.

Objective 4. Improve hydrodynamics module by improving terms used for physical drivers of migration dynamics in the model. We carefully designed the hydrodynamics module of *ePTM v2* to be fast, robust, and to represent the key processes revealed by our analyses. The steps taken to design and test this module are described in Section 4 and Appendix A.

Objective 5. Evaluate and validate the model's ability to robustly predict salmonid movements and fates across environmental conditions. Section 5 and Appendix A describe model evaluation steps taken to explore *ePTM v2* performance. In particular, the model performs well both in and out-of-sample.

6.3 Discussion of unmet objectives and future alternative approaches

The primary objectives of the study were met. Nevertheless, several secondary objectives were not completed to our satisfaction, in part due to data limitations. We discuss these below.

Interactions between salmonids and predators. Our analyses of predator-prey interactions focused on high-resolution, two-dimensional tracking studies from the Head of Old River region of the San Joaquin River (Section 3.3) because both predator and salmon tracking data were available in this region, and the domain size was tractable for CFD analyses (Olivetti *et al.* 2021). However, the degree to which we were able to explore direct predator-salmonid interactions across environmental conditions (e.g., flows) was limited by two factors: (1) the small overall number of predators detected within hydrophone arrays, and (2) the extremely small subset of data in which predators and salmonids co-occurred within the array at the same place and time. In the future, larger numbers of tagged predators and predator and smolt co-release schema might be used to address this data limitation.

Vertical movements of migrants in the water column. *ePTM v2* models movements of simulated migrants in channel-wise, cross-channel, and vertical dimensions of the water column. Our analyses of two-dimensional data sets yielded rich information about the behaviors of fish in channel-wise and cross-channel directions. However, depth measurements collected in two-dimensional hydrophone array studies were unreliable (AECOM 2015, S. Johnston personal communication). Future studies that resolve the depths at which migrants swim could address this gap in data availability.

Fine scale movements under strongly reversing tides. To our knowledge, two-dimensional hydrophone array studies in the Delta have only been conducted at the Head of Old River, Georgiana Slough, and Freeport, none of which typically displays the extreme reversing tides present in the most tidal regions of the system. Future studies that seek to resolve fine-scale salmonid movement behavior in these regions would be useful in informing future models.

Hydrodynamic representation at key channel junctions. Our analysis of the Chinook tracks at the Head of Old River allowed us to discover that in order to fully understand salmonid behaviors at local scales in complex flows, a nonhydrostatic CFD model is required. We therefore focused primarily on understanding such behavior dynamics, and discovered that the routing model currently in *ePTM v2*, itself based on laboratory flume-based flow profiles, does reasonably well in predicting routing probabilities. We will implement 3D flow-modeling in key channel junctions in the future.

6.4 Data and code delivery and management

Our analyses and model construction relied on analyses of previously published or otherwise publicly available data. These data sources, the code used in our analyses, and the *ePTM v2* model code are either already publicly available or provided in the following forms:

Olivetti et al. 2021:

Data. Data used in analyses are housed in a freely-available public repository on Dryad:
<https://doi.org/10.5061/dryad.2547d7wq4>

Code. Code is housed in a freely-available public repository on Dryad:
<https://doi.org/10.5061/dryad.2547d7wq4>

ePTM v2 model described in this report; Sridharan and Hein 2019:

Data. Data used in analyses described in this report are provided in several ways depending on whether the data source is already publicly accessible in the form in which it was used in our analyses. Chinook acoustic telemetry data used in the out-of-sample validation are available at: <https://oceanview.pfeg.noaa.gov/CalFishTrack/>. The San Joaquin River Group Authority conducted a 6-year steelhead tagging study from 2011-2016, and a portion of this dataset between 2011 and 2013 (SJRGA 2013) was made available to us by Rebecca Buchanan (Univ. Washington, Seattle). Two-dimensional Georgiana Slough datasets and ADCP data were supplied to us by Kate Le at California Department of Water Resources.

Code. Source code, model description, and model installation and instruction manuals are hosted in a public GitHub repository at: https://github.com/cvclcm/ePTM_v2

6.5 How project addressed Water Quality, Supply and Infrastructure Improvement Act of 2014, and 2016 California Water Action Plan

The project created knowledge and modeling tools relevant to stated objectives of the Water Quality, Supply and Infrastructure Improvement Act of 2014 (P1) and the 2016 California Water Action Plan (WAP2016) in the following ways:

- Create scientific knowledge and tools to inform restoration efforts of the San Joaquin River and inhabitant populations of salmon (relevant to “Bring Back Salmon to the San Joaquin River” WAP2016).
- Produce information and evaluation tools to identify key barriers to fish migration success. This objective is congruent with the WAP2016 and P1 Section 79732 objectives to remove barriers to fish migration (see “Eliminate Barriers to Fish Migration” WAP2016, P1 Section 79732).
- Make scientific results and modeling tools publicly available to promote cooperative voluntary and regulatory efforts as they relate to enhancement of Delta ecosystems (congruent with “Achieve Ecological Goals through Integrated Regulatory and Voluntary Efforts”, WAP2016).
- Inform efforts to assist in recovery of endangered and threatened migratory species (P1 Section 79732)
- Provide scientific knowledge and evaluation tools to enable adaptive management during extreme drought conditions (“Revise Operations to Respond to Extreme Conditions”, WAP2016)
- Provide calibrated and validated modeling framework capable of informing future coordination of water supply, flood control, hatchery operations, and restoration efforts in the Delta as they relate to salmon and steelhead (“Prepare for the Future Through Better Technology …”, WAP2016).
- Provide scientific knowledge to aid in restoring California rivers and watersheds to protect fish and wildlife corridors (P1 Section 79732).

6.6 Conclusions

The goal of this project was to use diverse data sources from the Delta, collected under different conditions and at several distinct spatial scales, to develop a mechanistic understanding of the salient processes that influence salmonid migration and survival through the Delta. We then sought to integrate this knowledge into a data-driven biological-hydrologic model capable of predicting salmonid migration patterns and survival through the system. These primary objectives were met and, as a result, we believe the *ePTM v2* model will provide an important tool for studying, managing, and forecasting salmonid migrations in the coming years.

7. REFERENCES

- AECOM, ICF International, and Turnpenny Horsefield Associates. 2015. An evaluation of juvenile salmonid routing and barrier effectiveness, predation, and predatory fishes at the Head of Old River.
- Anderson, J. J., Gurarie, E., & Zabel, R. W. (2005). Mean free-path length theory of predator-prey interactions: Application to juvenile salmon migration. *Ecological Modelling*, 186(2), 196-211.
- Berdahl, A., Westley, P. A., Levin, S. A., Couzin, I. D., & Quinn, T. P. (2016). A collective navigation hypothesis for homeward migration in anadromous salmonids. *Fish and Fisheries*, 17(2), 525-542.
- Buchanan, R. A., & Skalski, J. R. (2020). Relating survival of fall-run Chinook Salmon through the San Joaquin Delta to river flow. *Environmental Biology of Fishes*, 103(5), 389-410.
- Buchanan, R. A., Buttermore, E., Israel, J. 2020. Outmigration survival of a threatened steelhead population through a tidal estuary. *Can. J. Fish. Aquat. Sci.* 00: 1–18 (0000) dx.doi.org/10.1139/cjfas-2020-0467
- California Department of Fish and Wildlife (CDFW). 2018. Delta conservation framework: partnership and planning tools for 2050. Sacramento, CA.
- California Department of Water Resources (DWR). 1998. Methodology for flow and salinity estimates in the Sacramento-San Joaquin Delta and Suisun Marsh. Nineteenth Annual Progress Report to the State Water Resources Control Board.
- California Department of Water Resources (DWR). 2012. 2011 Georgiana Slough non-physical barrier performance evaluation final project report. Bay-Delta Office, Sacramento, California
- California Department of Water Resources (DWR). 2015a. 2012 Georgiana Slough non-physical barrier performance evaluation final project report. Bay-Delta Office, Sacramento, California
- California Department of Water Resources (DWR). 2015b. 2014 Georgiana Slough non-physical barrier performance evaluation final project report. Bay-Delta Office, Sacramento, California
- California Department of Water Resources (DWR). 2016. 2014 Georgiana Slough floating fish guidance structure performance evaluation project report. Bay-Delta Office, Sacramento, California
- California Department of Water Resources (DWR). 2020. California Data Exchange Center.
- Chapman, E. D., Hearn, A. R., Michel, C. J., Ammann, A. J., Lindley, S. T., Thomas, M. J., ... & Klimley, A. P. (2013). Diel movements of out-migrating Chinook salmon (*Oncorhynchus tshawytscha*) and steelhead trout (*Oncorhynchus mykiss*) smolts in the Sacramento/San Joaquin watershed. *Environmental Biology of Fishes*, 96(2), 273-286.
- Delta Stewardship Council. 2013. The Delta plan: ensuring a reliable water supply for California, a healthy Delta ecosystem, and a place of enduring value. Sacramento, CA.
- Delta Stewardship Council. 2019. Delta science plan: vision, principles and approaches for integrating and coordinating science in the Delta. Delta Science Program.
- Delta Stewardship Council. 2021a. Science action agenda 2022-2026: public review draft.
- Delta Stewardship Council. 2021b. Top Delta management questions.
- Demetras, N. J., Huff, D. D., Michel, C. J., Smith, J. M., Cutter, G. R., Hayes, S. A., and Lindley, S. T. 2016. Development of underwater recorders to quantify predation of juvenile Chinook salmon (*Oncorhynchus tshawytscha*) in a river environment. *Fisheries Bull.* 114:179–185
- Gross, E. S., Holleman, R. C., Thomas, M. J., Fangue, N. A., & Rypel, A. L. (2021). Development and Evaluation of a Chinook Salmon Smolt Swimming Behavior Model. *Water*, 13(20), 2904.
- Hance, D. J., Perry, R. W., Burau, J. R., Blake, A., Stumpner, P., Wang, X., & Pope, A. (2020). Combining Models of the Critical Streakline and the Cross-Sectional Distribution of Juvenile Salmon to Predict Fish Routing at River Junctions. *San Francisco Estuary and Watershed Science*, 18(1).
- MacFarlane, R. B., & Norton, E. C. (2002). Physiological ecology of juvenile chinook salmon (*Oncorhynchus tshawytscha*) at the southern end of their distribution, the San Francisco Estuary and Gulf of the Farallones, California. *Fishery Bulletin*, 100(2), 244-257.
- Michel, C. J., Ammann, A. J., Lindley, S. T., Sandstrom, P. T., Chapman, E. D., Thomas, M. J., ... & MacFarlane, R. B. (2015). Chinook salmon outmigration survival in wet and dry years in California's Sacramento River. *Canadian Journal of Fisheries and Aquatic Sciences*, 72(11), 1749-1759.
- Michel, C. J., Notch, J. J., Cordoleani, F., Ammann, A. J., & Danner, E. M. (2021). Nonlinear survival of imperiled fish informs managed flows in a highly modified river. *Ecosphere*, 12(5), e03498.
- Michel, C.J., Henderson, M.J., Loomis, C.M., Smith, J.M., Demetras, N.J., Iglesias, I.S., Lehman, B.M. and Huff, D.D., 2020. Fish predation on a landscape scale. *Ecosphere*, 11(6), p.e03168.
- National Marine Fisheries Service (NMFS). 2014. Recovery plan for the evolutionarily significant units of Sacramento River Winter-run Chinook salmon and Central Valley Spring-run Chinook salmon and the distinct

- population segment of California Central Valley steelhead. West Coast Region. Sacramento, CA. 1561 p. Available at: https://media.fisheries.noaa.gov/dam-migration/central_valley_salmonids_recovery_plan-accessible.pdf
- Notch, J. J., McHuron, A. S., Michel, C. J., Cordoleani, F., Johnson, M., Henderson, M. J., & Ammann, A. J. (2020). Outmigration survival of wild Chinook salmon smolts through the Sacramento River during historic drought and high water conditions. *Environmental Biology of Fishes*, 103(5), 561-576.
- Notch, J., R. Robinson, T. Pham, R. Logston, A. McHuron, A. Ammann, C. Michel. 2021. Enhanced Acoustic Tagging, Analysis, and Real-Time Monitoring of Wild and Hatchery Salmonids in the Sacramento River Valley – 2018 - 2020 Final Report. Report prepared by University of California – Santa Cruz for the U.S. Bureau of Reclamation under contract USDI/BOR# R18AC00039.
- Olivetti, S, VK Sridharan, MA Gil, AM Hein. 2021. Merging computational fluid dynamics and machine learning to reveal animal migration strategies. *Methods Ecol. Evol.* DOI: 10.1111/2041-210X.13604
- Perry, R. W., Pope, A. C., Romine, J. G., Brandes, P. L., Burau, J. R., Blake, A. R., ... & Michel, C. J. (2018). Flow-mediated effects on travel time, routing, and survival of juvenile Chinook salmon in a spatially complex, tidally forced river delta. *Canadian Journal of Fisheries and Aquatic Sciences*, 75(11), 1886-1901.
- Perry, R. W., Pope, A. C., Romine, J. G., Brandes, P. L., Burau, J. R., Blake, A. R., ... & Michel, C. J. (2018). Flow-mediated effects on travel time, routing, and survival of juvenile Chinook salmon in a spatially complex, tidally forced river delta. *Canadian Journal of Fisheries and Aquatic Sciences*, 75(11), 1886-1901.
- Perry, R. W., Romine, J. G., Adams, N. S., Blake, A. R., Burau, J. R., Johnston, S. V., & Liedtke, T. L. (2014). Using a non-physical behavioural barrier to alter migration routing of juvenile chinook salmon in the Sacramento–San Joaquin River delta. *River Research and Applications*, 30(2), 192-203.
- Perry, R. W., Skalski, J. R., Brandes, P. L., Sandstrom, P. T., Klimley, A. P., Ammann, A., & MacFarlane, B. (2010). Estimating survival and migration route probabilities of juvenile Chinook salmon in the Sacramento– San Joaquin River Delta. *North American Journal of Fisheries Management*, 30(1), 142-156.
- San Joaquin River Group Authority. 2013. On implementation and monitoring of the San Joaquin River agreement and the Vernalis Adaptive Management Plan (VAMP). 2011 Annual Technical Report.
- Sridharan, V. K., and Hein, A. M. 2019. Analytical solution of advection-dispersion boundary value processes in rivers and estuaries. *Water Resources Research*, 55 (12).
- Sridharan, V. K., Monismith, S. G., Fong, D. A., & Hench, J. L. (2018). One-dimensional particle tracking with streamline preserving junctions for flows in channel networks. *Journal of Hydraulic Engineering*, 144(2), 04017063.
- Sridharan. 2018. Matlab toolbox for automatic clean-up of coastal and estuarine tidal datasets. Fall Meeting of the American Geophysical Union, San Francisco, CA.
- Stumpner, P. n.d. a. Head of Old River 2012 ADCP deployment memo, AECOM Ltd.
- Stumpner, P. n.d. b. Georgiana Slough 2012 ADCP deployment memo, AECOM Ltd.
- Stumpner, P. n.d. c. Georigana Slough 2014 ADCP deployment memo, AECOM Ltd.
- Wang, R.F., Ateljevich, E., Fregoso, T.A., and Jaffe, B.E. (2018). A revised continuous surface elevation model for modeling.” In: Methodology for Flow and Salinity Estimates in the Sacramento-San Joaquin Delta and Suisun Marsh: 39th Annual Progress Report. Bay-Delta Office, California Department of Water Resources and Pacific Coastal and Marine Science Center, United States Geological Survey, pp. 125–170.

FIGURES

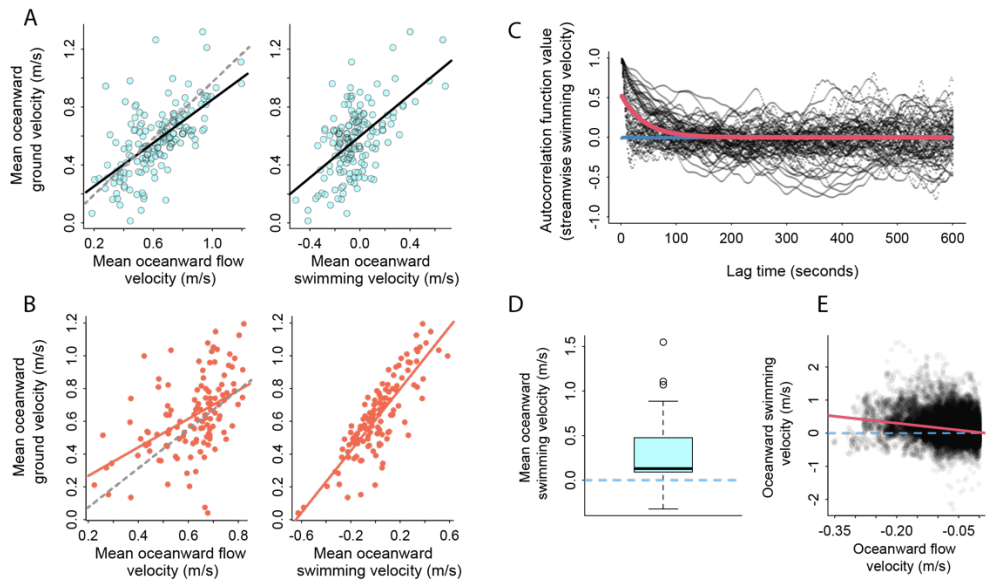


Figure 3.2.1: Fine-scale movements of Chinook salmon and steelhead. **(A)** Mean (by individual fish) oceanward ground velocity as a function of oceanward flow (left) and mean oceanward swimming velocity (right) flow for late-fall run Chinook and **(B)** steelhead at the Georgiana Slough junction on the Sacramento River in 2012 (DWR 2015a). Note positive correlations between mean ground velocity and mean oceanward flow for both species, and strong positive correlations between mean ground velocity and mean oceanward swimming velocity for both species. Dashed line is 1:1 line. **(C)** Swimming velocity autocorrelation function values as a function of lag time, computed for late-fall run Chinook at the Georgiana Slough junction in 2012 (DWR 2015a). Black lines show values for individual fish. Red line is an exponential fit to all fish. Average temporal autocorrelation decays within 1-2 minutes; however some individual fish show persistent temporal autocorrelation for significantly longer periods of time. **(D)** Mean oceanward swimming velocity of late-fall Chinook during periods of tidal flow reversal (Georgiana Slough, 2014; DWR 2015b) showing positive oceanward swimming velocities. **(E)** Individual swimming velocity observations from late-fall Chinook during tidal flow reversal (data as in (D)) showing stronger oceanward swimming velocity under stronger landward tidal flows (i.e., oceanward flow < 0). In all panels, only periods in which the bio-acoustic fish fence was off were included in analyses (DWR 2015a; 2015b).

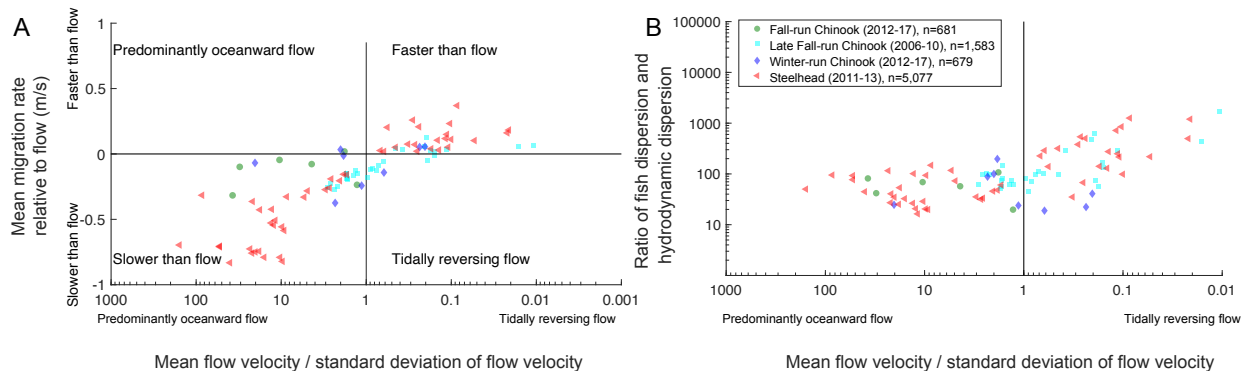


Figure 3.2.2: Salmonid population movement patterns through Delta reaches. (A) mean relative migration rate (mean migration rate – mean flow velocity) for all release groups of fish through Delta reaches as a function of the ratio of the mean water velocity to the standard deviation in water velocity over the period of reach entry. Values below zero indicate average migration rates slower than mean flow. Values greater than zero indicate average migration rate faster than mean flow. Note that the horizontal axis is reversed (i.e. large values on left, small values on right) to correspond to the progression migrants typically experience as they move from more riverine (left) to more tidal (right) regions of the Delta. (B) The ratio of the dispersion coefficient calculated from travel times of individual fish within a release group to the flow-dependent hydrodynamic dispersion scale (vertical axis). This relative measure is expressed as function of the ratio of the mean water velocity to the standard deviation in water velocity over the period of reach entry as in (A). Ratio of 1 would indicate equality between observed dispersion and hydrodynamic dispersion. Observed values indicate that rate of spreading of fish exceeds hydrodynamic dispersion by a factor of 10-1,000. Note also increasing value of ratio for strongly tidal conditions (i.e., right half of plot). Legend shows run / species, source of data, year range, and number of data points included.

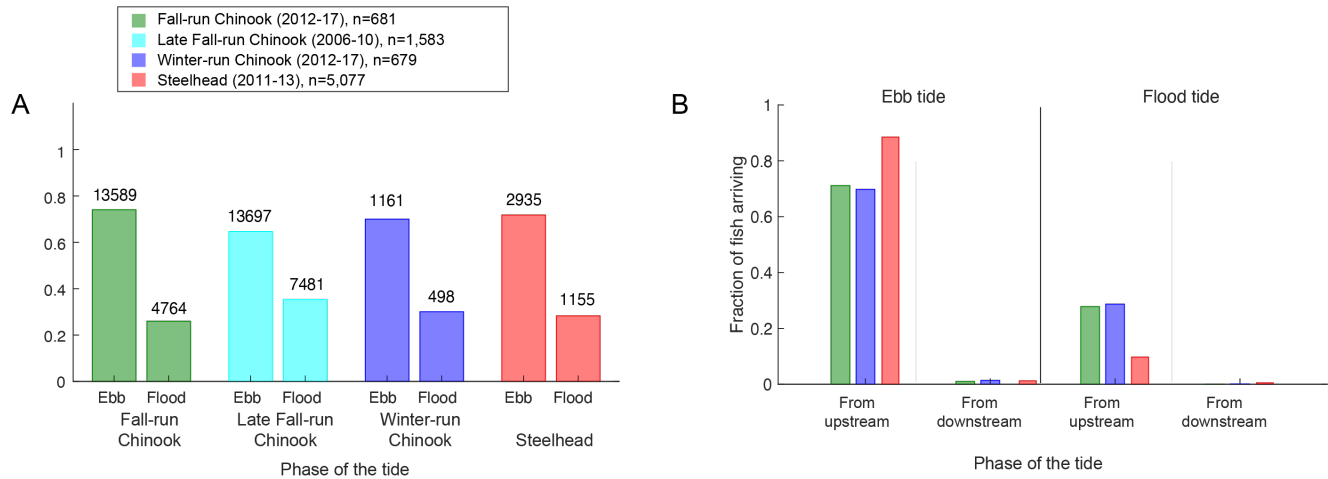


Figure 3.2.3: Arrival patterns in strongly tidal Delta regions. (A) Fraction of arrivals during flood and ebb tides for different runs/species. Note for all runs, arrivals are strongly biased toward ebb (i.e. outgoing) tides. (B) Patterns of arrivals by origin (upstream or downstream), showing majority of arrivals are from upstream during both ebb (outgoing) and flood (incoming) tides, consistent with the hypothesis that fish resist being pushed landward by incoming tidal flow in reversing tidal regions.

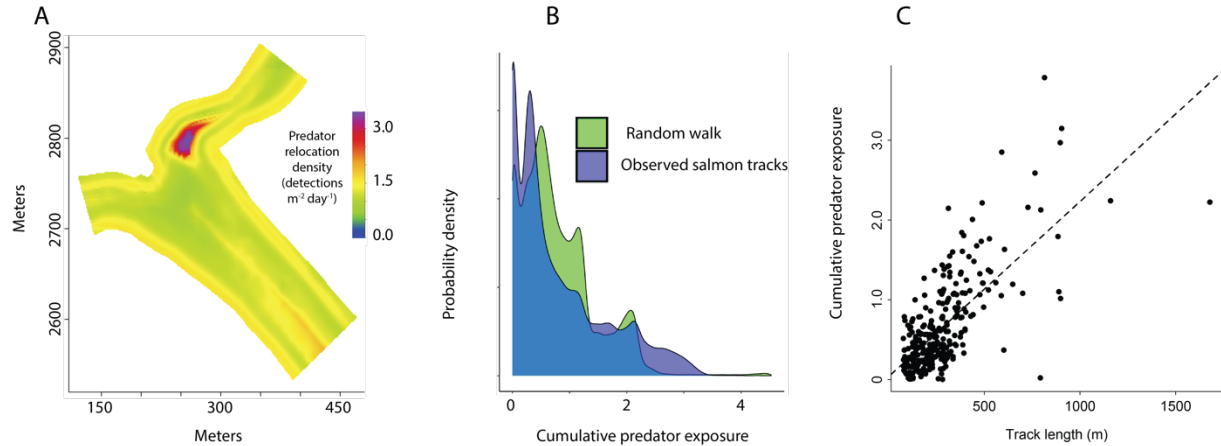


Figure 3.3.1: Predation risk in space: (A) Predator density landscape at Head of Old River. Computed from predator relocations. (B) Distribution of predator exposure values integrated over observed salmon tracks (blue) and paired random walks (green). (C) Relationship between track length and exposure for tracks longer than 75 m in length, showing positive correlation between track length and exposure. Note that this correlation need not exist *a priori*. For example, if fish systematically avoided high predator density regions, one would not necessarily expect a positive correlation between track length and exposure.

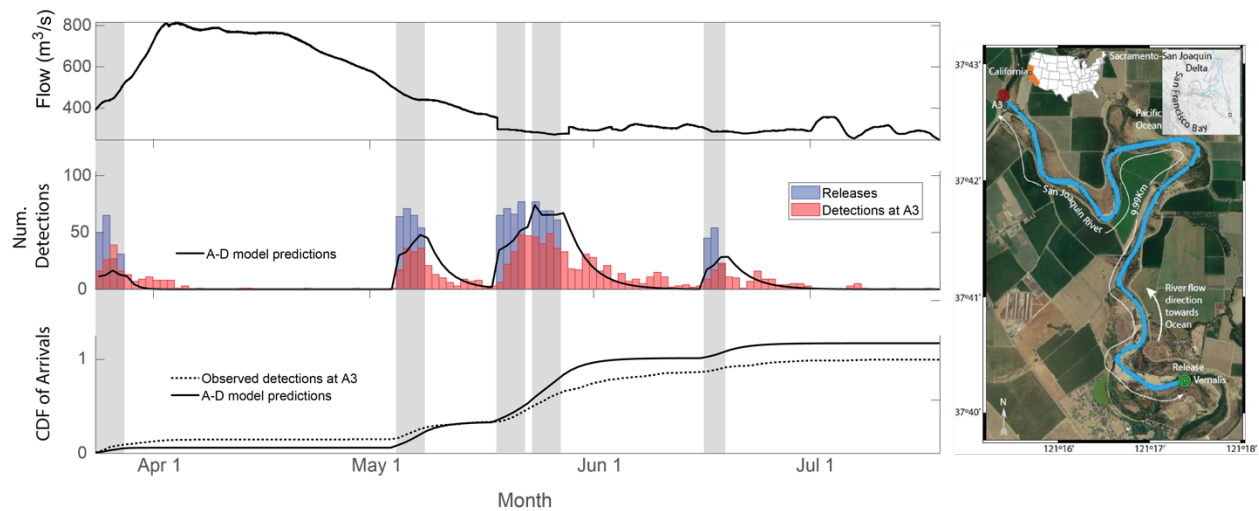


Figure 3.4.1: Population movement patterns and Advection-Dispersion models: Sridharan and Hein (2019) applied a one-dimensional Advection-Dispersion model to steelhead acoustic telemetry data in the San Joaquin River. Map shows study region (described in Buchanan et al. 2020, and Sridharan and Hein 2019). Upper plot shows discharge near Vernalis, CA over the study period. Middle plot shows releases (in blue) and acoustic receiver detections at the hydrophone station at A3 (red, see inset map). Black line shows prediction of Advection-Dispersion model assuming distributed release and absorbing boundary at the receiver array (Sridharan and Hein 2019). Lower plot shows observed (dashed line) and predicted (solid line) cumulative distribution function (CDF) of detections across all releases.

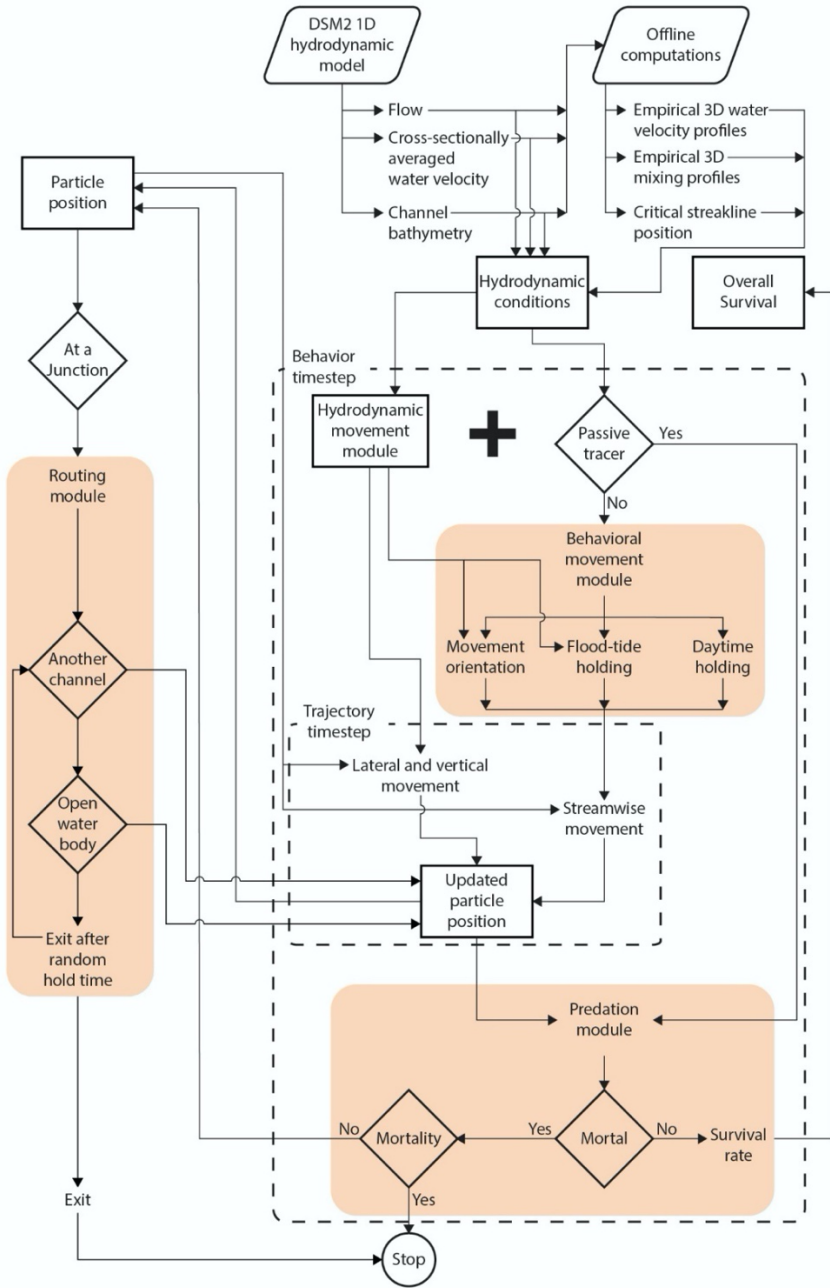


Figure 4.1.1: ePTM v2 model structure. Model inputs shown in parallelograms. Model outputs shown in rectangles. Decision points shown in rhombuses. The three key biological processes are highlighted. The dashed boxes indicate the biological timestep and trajectory sub-timestep respectively. The key processes occur over each timestep to update a simulated particle's position. Model computations stop when a particle either dies or exits the system.

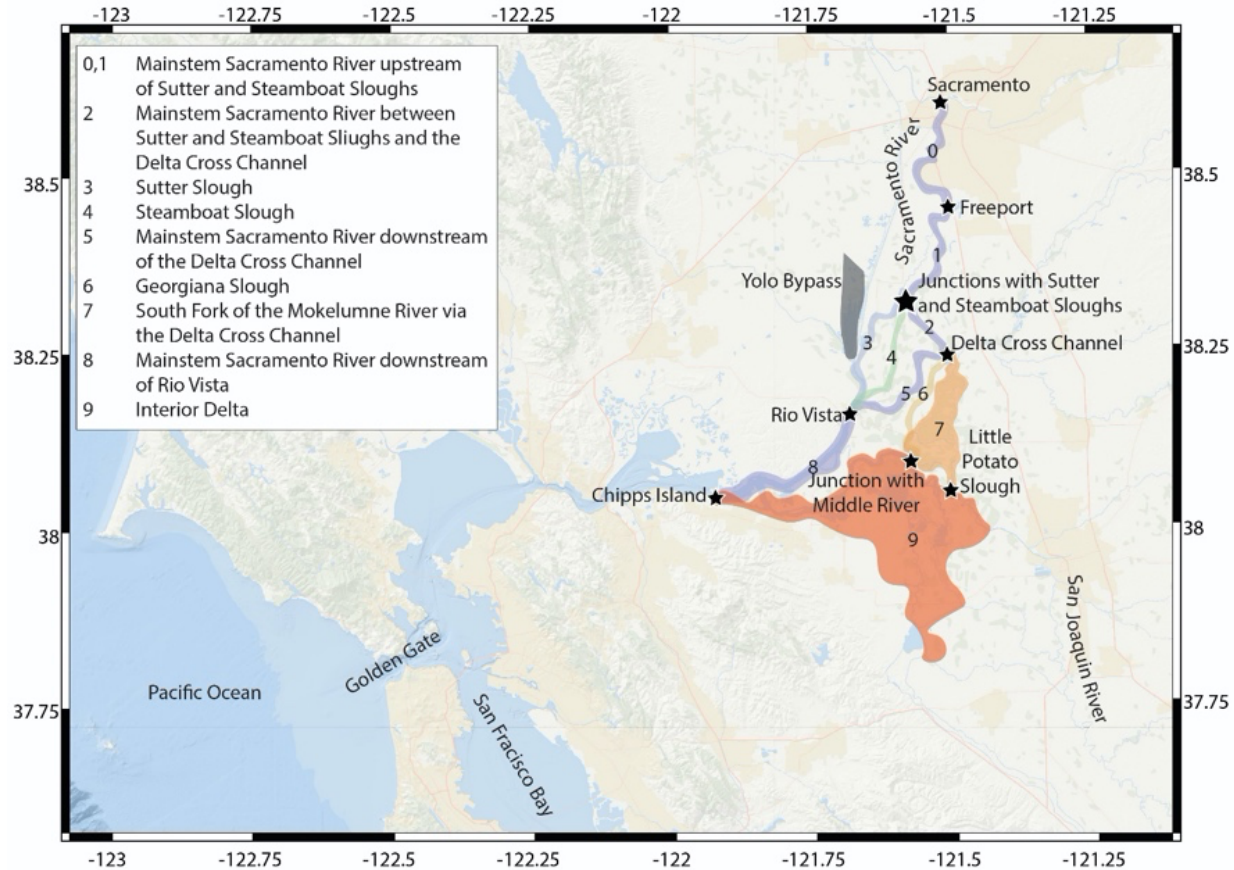


Figure 5.1.1: Delta reaches. Delta reaches defined in previous analyses of late fall Chinook acoustic tagging data (Perry *et al.* 2010; Perry *et al.* 2018).

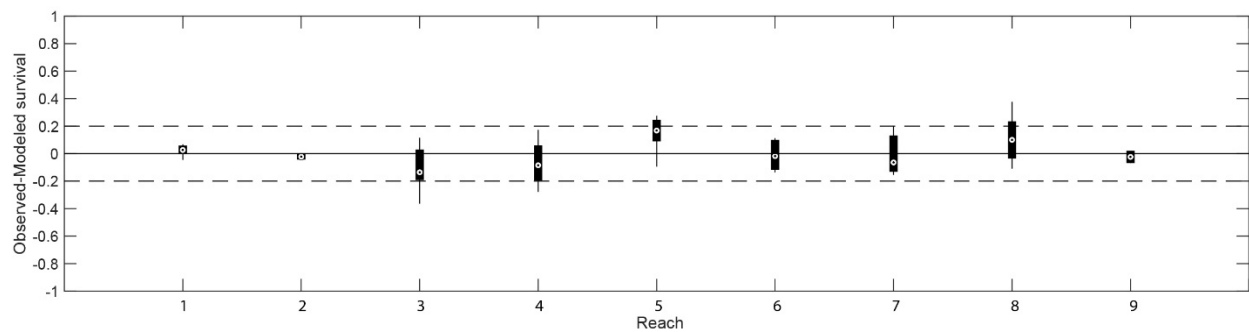


Figure 5.1.2: Survival estimates. Deviation of predicted survival from observed survival measured as observed – predicted survival. The boxplots include estimates of survivals for all release group using the best performing twenty survival parameter sets in each reach. A value of zero indicates a perfect match between observation and prediction. Reach numbers correspond to those shown in Figure 5.1.1.

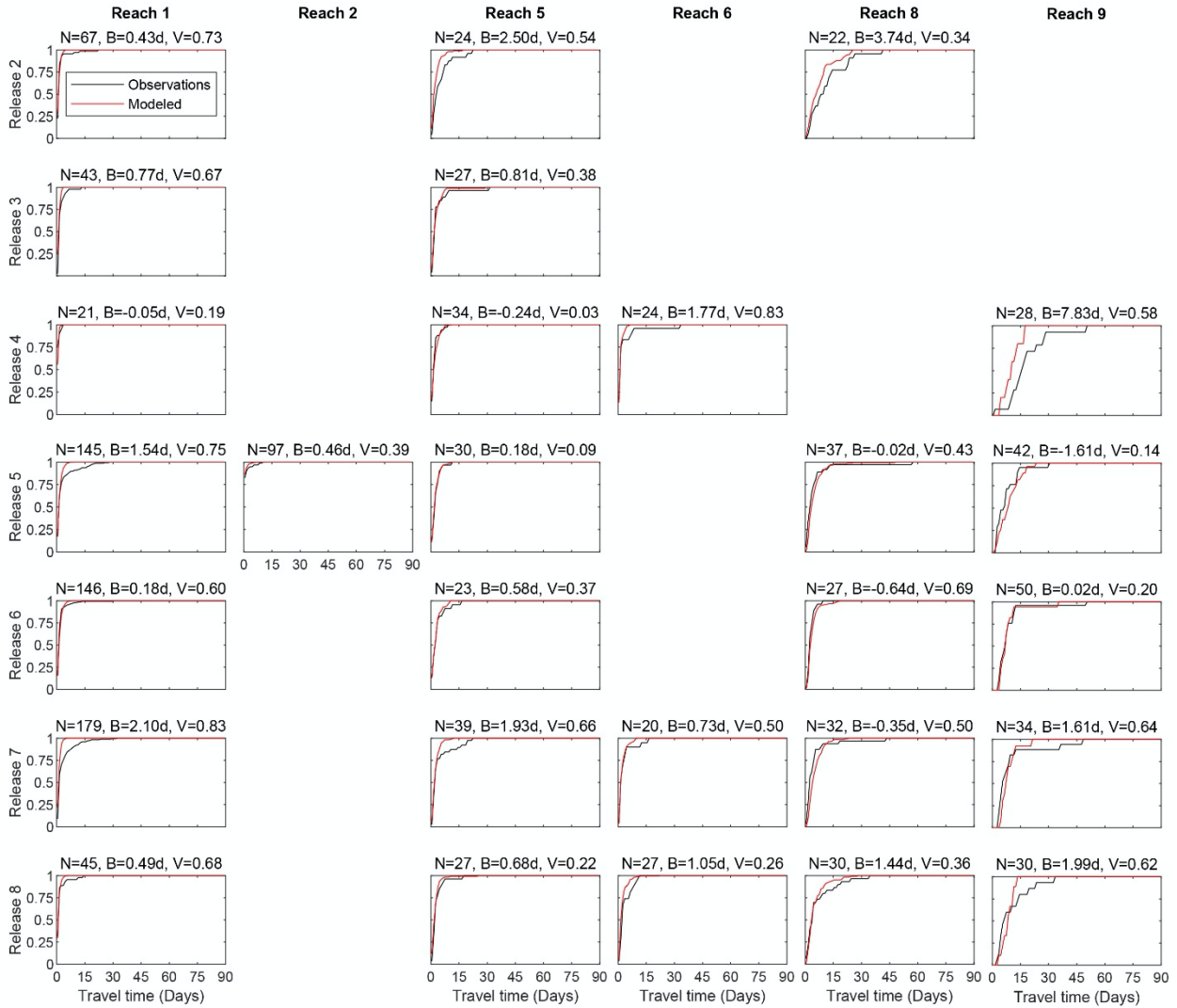


Figure 5.1.3: Travel time estimates. Observed and predicted cumulative distributions of travel times for late-fall run Chinook. Rows indicate release groups and columns indicate reaches. In each plot, N indicates the number of fish, B indicates the signed bias between the observed and modeled mean travel times, and V indicates by how much the standard deviation in predicted travel times vary relative to the standard deviation in observed travel times. Only reaches with at least 20 fish that were detected at both the upstream and downstream ends of the reach are shown. Reach numbers as in Fig. 5.1.1.

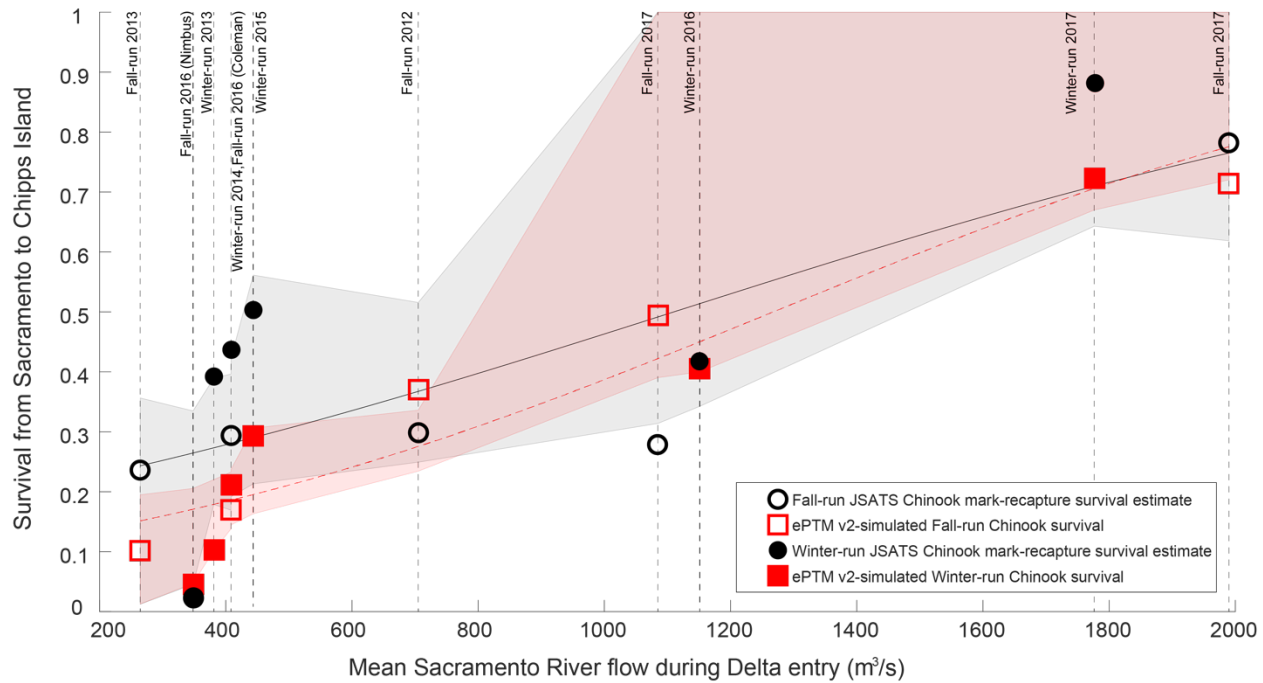


Figure 5.2.1: Comparison between ePTM v2 predictions and observed survival in out-of-sample data. Red squares represent model predictions and black circles represent CJS estimates fit to the data. Open symbols indicate fall run and closed symbols indicate winter run releases. For each release, flows were estimated as the mean flow in the Sacramento River at Freeport over the duration between the first fish passage and the last fish passage through this location. The dashed red line and black solid line represent a logistic curve fit to the model results and the CJS-reported survivals. Red and grey shaded areas represent 95% confidence intervals generated by applying the same logistic fit to 10,000 replicates of these points chosen at random with replacement.

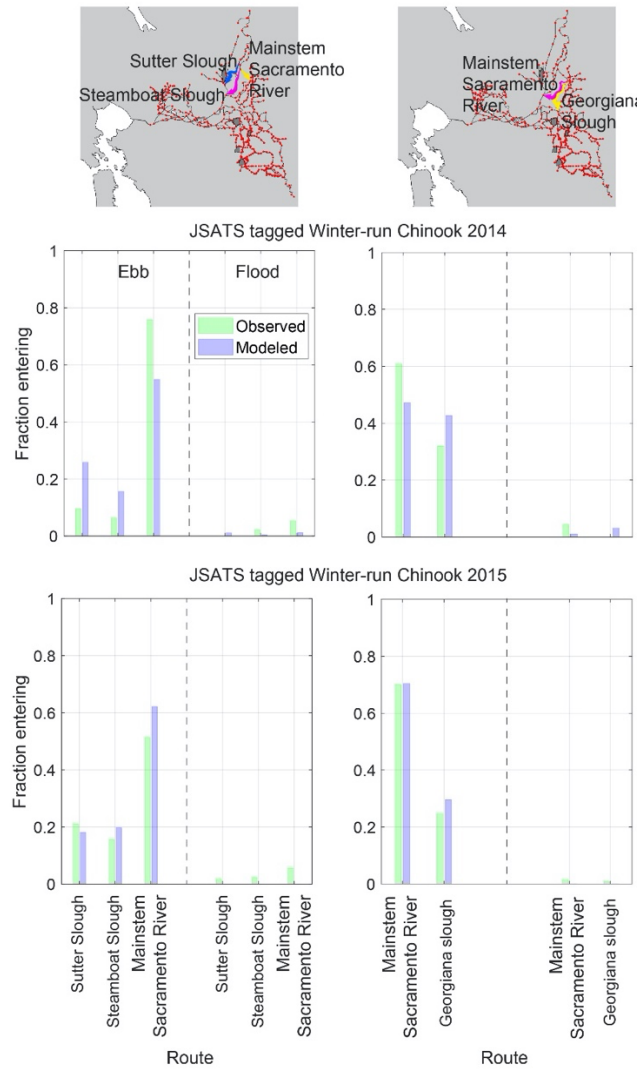


Figure 5.2.2: Comparison between ePTM v2 predictions and observed route use in out-of-sample data. Green bars indicate fraction of total Chinook passing through telemetry stations in the different routes. Blue bars indicate ePTM predictions of fraction of particles passing through equivalent nodes on the DSM2 grid. Passage fractions are aggregated over different phases of the tide at two key junctions that are important to overall survival in the Delta: the Mainstem Sacramento River with diversions to Sutter and Steamboat Sloughs on the left, and the Mainstem Sacramento River and Georgiana Slough on the right. The top panels provide visual guides superimposed on the DSM2 grid map to orient the reader. In both out-of-sample years, the patterns of route use observed in the Data are predicted reasonably well by the model. In 2014, a floating fish guidance structure was in place upstream of Georgiana Slough, and this has been represented in the model with a barrier efficiency of 77.7% reported in DWR (2016).

APPENDICES

APPENDIX A. Structure, Formulation, Calibration, and Evaluation of the Enhanced Particle Tracking Model Version 2 (*ePTM v2*)

Like its predecessor, the NOAA-UCSC enhanced particle tracking model, *ePTM v2* is a coupled physical-biological Lagrangian particle tracking model that simulates the movements and mortality of juvenile salmonids in the Delta. While they can be computationally intensive, the advantage of such Lagrangian models is the relative ease of specifying different behaviors one wishes simulated particles to follow, and the simplicity of separating model components in a modular way. For example, in *ePTM v2*, velocity of fish due to active swimming locomotion and water velocity combine additively to determine fish ground velocity (see also Olivetti *et al.* 2021), a feature that makes it easy to modify assumptions about physical forcing by water, the processes that determine locomotion, or both. Moreover, because the model simulates the movements of individual fish, each of which uses stochastic behavioral rules to produce behavior and is subject to stochastic mortality, model runs that simulate populations of migrants naturally provide distributions of output values: for example distributions of travel times or locations where mortality events occur.

The structure of *ePTM v2* is designed to simulate three key processes related to salmonid migration through the Delta, which are illustrated in Figure 4.1.1 of this report. These processes are (1) within channel movements, (2) routing at channel junctions, and (3) mortality due to predators. At each simulation timestep, simulated migrants move through the channel where they are located, experience a probability of mortality due to predation, and, if they are in the vicinity of a channel junction, move into one downstream channel or the other. By iterating this process over many timesteps, *ePTM v2* generates predictions about how populations of simulated migrants move through the Delta, and when and where mortality occurs. The following sections provide a detailed account of how these processes are simulated to produce model predictions.

Simulation timescales. The *ePTM v2* model simulates processes with two distinct but fixed time step sizes. The primary timestep, τ , is 15 minutes. Every τ units of time, migrant behaviors are updated and mortality is evaluated. The 15 minute timestep represents a compromise between resolving fast timescale processes, and the computational cost of simulating movements and behaviors of thousands of migrants for simulated periods of time ranging from days to weeks, and the desire to enable simulations over hundreds or thousands of current and future scenarios. Balancing this trade-off is essential, given that typically, over an eighty-year water management scenario, nearly 20 million fish are simulated.

Given the 15 minute timestep, fish behaviors in *ePTM v2* should be interpreted as temporally coarsened versions of the fast timescale processes that occur on the timescale of seconds and spatial scale of meters (see Olivetti *et al.* 2021 for an example of analyses addressing this finer scale). While changes in migrant behavior are simulated over these coarser time intervals, changes in migrant position can be updated at manageable computational cost on a timescale shorter than the primary timestep. In particular, we simulate changes in migrant position and routing decisions, when necessary, on a sub-timestep, Δt , of 20 seconds. This finer time resolution helps resolve things like movements relative to flows in bent channels and total path length through a reach during a 15 minute interval.

A1.1 Within-channel movements

As discussed above, the hydrodynamic and locomotion components of within-channel movements are additive. This means that they can be decoupled so that hydrodynamics and locomotion remain modular and customizable species or runs. This additivity also allows us to write the overall migration velocity of a given individual in a timestep as, $= u_L + u_H$, where u is migration velocity expressed as the rate of movement through the channel in the oceanward direction (i.e., $u > 0$ is oceanward movement and $u < 0$ is landward movement), u_L is fish locomotion velocity, and u_H is the hydrodynamic velocity of the water the fish is moving in. At any given timestep, u_L , is set by the swimming behavior of the simulated migrant, whereas u_H is determined by hydrodynamic simulations of the flow through the Delta. The latter quantity is computed through hydrodynamic simulations from the 1D shallow-water equation solver, DSM2 (DWR 1998). The following two subsections describe how the swimming component of movements and hydrodynamic component of movements are computed in the model.

A1.1.1 Swimming locomotion:

Swimming locomotion in *ePTM v2* involves a sequence of behavioral “choices” each migrant makes at each simulation timestep. As noted above, these should be interpreted as coarsened representations of the fine scale swimming behaviors exhibited by migrants, which can vary in space, time, and among individual migrants (Olivetti et al. 2021, Section 3).

We capture these behaviors using a hierarchy of stochastic behavioral decisions. At each simulation timestep, the sequence of behavioral choices involves the following hierarchy:

- (I) hold or swim,
if swim
- (II) select swimming direction
- (III) select swimming speed.

The outcome of these behavioral decisions at each timestep are stochastic, and they are produced by a set of behavioral functions that provide the probabilities of each action based on the physical conditions and location of the animal. The forms of functions are selected based on empirical evidence from our analyses of salmonid migration behavior in the Delta (Section 3), acknowledging that some simplifying assumptions are necessary to ensure that parameters are statistically identifiable and that computation times during model runs are kept within an acceptable range. Evidence for each behavioral decision and its functional representation is given in the sections below.

I. Hold or swim. Several environmental factors have been observed to determine whether migrants swim actively in a given time period or exhibit “holding” behavior, during which their movements are minimal (Chapman et al. 2013; Michel et al. 2015). For example, during reversing flood tides holding-like behavior is evident in the long durations of residence of migratory steelhead in the vicinity of acoustic telemetry arrays, as well as the very low proportion of total arrivals at hydrophone arrays during reversing flood tides (Section 3, Fig. 3.2.3). A second factor observed to determine whether juvenile salmonids move or hold position is phase of the diel cycle. Chapman et al. (2013) reported that the proportion of fish detected during the daytime versus the nighttime varied as a function of where they were in the Sacramento River and the Delta from 10% to 75%. They also showed that the proportion of fish arriving during different photoperiods became more comparable further oceanward into the system between the River and the Delta. We note that the term “holding” might be taken to imply that fish do not move; however, our analyses of fine-scale movements and arrival timings of juvenile Chinook and steelhead suggest that time periods in which fish are completely stationary are rare (Olivetti et al. 2021). Rather, fish commonly exhibit cross-channel and

streamwise meanders, and locomotion force production directed against flow. The net effect of such actions on the timescale of tens of minutes to hours is to significantly slow the rate at which migrants move oceanward (Section 3, Fig. 3.2.2). To retain simplicity, we refer to such behaviors as “holding” and assume that, on average, fish in the holding state do not progress either oceanward or landward during a simulation timestep.

In *ePTM v2*, whether a fish will hold or swim during a given simulation timestep is determined by two factors: the flow velocity at the migrant’s location u_H , and the phase of the diel cycle (flood tide or ebb tide). These dependencies are implemented by the following equations

$$P(\text{hold}) = \begin{cases} p_H, & \text{if } u_H < u_F \\ \mathbf{I}_{t \in \{D\}}(1 - p_{DS}), & \text{otherwise} \end{cases} \quad \dots(\text{A1})$$

, where, p_H is a probability that the fish holds, u_F is a flow threshold below which fish are assumed to hold position, $\mathbf{I}_{t \in \{D\}}$ is an indicator function denoting whether it is day ($\mathbf{I}_{t \in \{D\}} = 1$) or night ($\mathbf{I}_{t \in \{D\}} = 0$), and p_{DS} is the probability of swimming during the daytime (Chapman *et al.* 2013). If $1 > P(\text{hold}) > 0$, the migrant’s decision to hold is determined by a Bernoulli trial with probability $P(\text{hold})$. The hydrodynamic flow condition given in the upper expression on the right hand side of Equation (A1), reflects the observed behavior described above whereby fish moving in tidal regions of the Delta stop advancing and remain in a local region during strong incoming tides that cause the flow to reverse. For example, setting $u_F = 0$ implies that fish experiencing landward flow during a flood tide (i.e., $u_H < 0$) will hold position with probability p_H rather than move in the flow. In practice, we treat the three parameters that affect the decision to hold at any given timestep, u_F , p_H and p_{DS} (Table 1) as free parameters. This allows the model to capture different types of holding behavior observed in the system, and also allows us to represent the holding behavior as a fuzzy rule rather than as a hard cutoff.

The choice to hold or not to hold is evaluated for each simulated fish at each timestep. If a fish holds, it is assumed that the animal is neither moving via active locomotion nor via forcing by the flow, and therefore the migrant’s ground speed is $u(x, t) = 0$. As discussed above, a migrant could accomplish this type of behavior if, for example, it were to actively swim against flow leading to a net zero ground speed (Olivetti *et al.* 2021), or if it were to shelter from flow in submerged structure or in the flow boundary layer at the channel bottom or banks (e.g., Liao 2007).

II. Swimming direction. In the Delta, the direction of swimming relative to flow varies across the system and over environmental conditions (Section 3, Olivetti *et al.* 2021). To incorporate this into *ePTM v2*, we incorporate a probabilistic swimming direction rule that determines each migrant’s swimming direction at each timestep. The structure of this rule is based on two empirical patterns evident in analyses of salmonid migrations in the delta. Firstly, while migrants do regularly turn within the channel, directing locomotion landward, oceanward, or toward channel banks, they also exhibit a tendency to persist in a given swimming direction for a period of time (Section 3, Olivetti *et al.* 2021). To capture this tendency to move in a persistent locomotion direction, we assume that at each simulation timestep, a fish persists in its previous swimming direction (i.e., either oceanward, or landward) with probability p_M . The decision to persist is then determined by a Bernoulli distribution with probability p_M .

If the Bernoulli draw to determine persistence results in a zero, the fish’s swimming direction is determined by a stochastic decision based on the flow it experiences during the current timestep. This is motivated by the observation that fish in different flow regimes exhibit different tendencies to swim with or against prevailing flow (Olivetti *et al.* 2021). Fish could measure flow through a range of processes including lateral line-mediated flow sensing (Liao 2007, Oteiza *et al.* 2017), and optical

flow-based perception of relative flow (Miles et al. 2021). We do not attempt to determine the mechanism through which flow is perceived, however, we note that very weak flows are difficult to perceive regardless of the sensory mechanisms, and are thus unlikely to influence swimming direction, whereas strong flows are easier to perceive. A simple way to represent this is to model the probability of orienting in the direction of prevailing flow as a function of the dimensionless water velocity magnitude,

$$\tilde{u} = |u_H|/|\bar{u}| \quad \dots \text{(A2)}$$

where $|u_H|$ is the water velocity magnitude at the migrant's location and $|\bar{u}|$ is the historical average velocity of flow in the Delta. The quantity $|\bar{u}|$ serves simply to normalize u^* to a consistent range of values and any other constant could be used in its place without loss of generality (i.e., we are not assuming a fish has knowledge of the historical average water velocity). We assume water velocity magnitude is related to the fish's probability of orienting in the direction of the prevailing flow according to the function:

$$p_{SWF}(t) = 0.5 + (P_{System} - 0.5) \left[\frac{1}{1+e^{(-c-\beta \log \tilde{u})}} \right], \quad \dots \text{(A3)}$$

where p_{SWF} is the probability of orienting in the direction of flow, P_{System} is a calibrated constant determined by where the migrant is located in the system, c is the logistic half saturation constant, and β is the logistic slope parameter. If a fish is not holding, and not persisting in its previous movement direction, its direction is determined by a Bernoulli draw with probability given by $p_{SWF}(t)$ from Equation (A3), where success indicates that locomotion is oriented in the same direction as the prevailing flow, and failure indicates that it is directed against the prevailing flow. The free parameters involved in selecting swimming direction are P_{System}, c, β , and p_M (Table A1). The P_{System} parameter and the sign of β determine how the probability of swimming with flow changes as flow magnitude changes. By allowing these parameters to vary in different regions of the system, spatial variation in responses to flows (Section 3) can be captured.

III. Swimming speed. The final component of locomotion behavior is swimming speed. Swimming speeds of migratory salmonids in the Delta vary over time, across environmental conditions, and in different regions of the Delta (Section 3, Olivetti et al. 2021). To allow swimming speed to vary from one timestep to another and among migrants, we draw a random swimming speed for each simulated fish that is not holding at each point in time. The swimming speed, $|u_L|$, for each simulated fish at each timestep is drawn from a log-normal distribution of the form

$$\ln N(\mu, \sigma) \sim \frac{1}{|u_L| \sigma \sqrt{2\pi}} e^{-\left[\frac{(\ln |u_L| - \mu)^2}{2\sigma^2} \right]} \quad \dots \text{(A4)}$$

where the parameters are given by

$$\begin{aligned} \mu &= 2 \ln |\bar{u}_S| - \frac{1}{2} \ln (\sigma_{|u_S|}^2 + |\bar{u}_S|^2) \\ \sigma &= \sqrt{\ln (\sigma_{|u_S|}^2 + |\bar{u}_S|^2) - 2 \ln |\bar{u}_S|} \end{aligned} \quad \dots \text{(A5)}$$

in which the mean swimming speed and standard deviation in observed swimming speeds are respectively $|\bar{u}_S|$ and $\sigma_{|u_S|}$. To remain consistent with the finding that salmonid swimming behavior changes over the course of migration (Section 3), we allow the parameters of the log-normal distribution for swimming speed to vary among reaches or regions (e.g., riverine, transitional, reversing tidal reaches) as fish move through the Delta. To ensure that randomly drawn swimming

speeds remain within the range of biologically plausible speeds, the log-normal distribution is truncated at the 95th percentile and rescaled appropriately. Free parameters involved in selecting migration speeds are $\bar{|u_S|}$ and $\sigma_{|u_S|}^2$ (Table A1).

Table A1. *ePTM v2* swimming behavior parameters

Locomotion component	Description	Fitting parameters
Active swimming	Swimming speed	$\bar{ u_S }, \sigma_{ u_S }^2$
Swimming direction	Probability of swimming with the flow	$c, \beta, p_M, P_{System}$
Holding behavior	Holding threshold	u_F
	Daytime swimming probability	p_{DS}
	Holding probability above threshold	p_H

A1.1.2 Hydrodynamics and physical forcing on fish:

The hydrodynamic components of migrant ground velocity is computed using the 1D shallow-water equation solver, *DSM2* (DWR 1998). Although the positional variable of primary interest is the location of each migrant along the channel, $x(t)$, we represent the location of each migrant at each time in three dimensions – $x(t)$, $y(t)$, and $z(t)$ – where $y(t)$ is the animal's location in the cross-channel dimension, and $z(t)$ is the animal's location in the vertical dimension. $y(t)$ is specified as positive from the channel centerline to the right bank looking downstream, and $z(t)$ is specified as positive from the channel bottom to the free surface. At each sub-timestep, Δt , positions are updated according to the following equations:

$$\begin{aligned} x(t+1) &= x(t) + [u_H + u_L] \Delta t \\ y(t+1) &= y(t) + R_y \sqrt{2\varepsilon_H \Delta t} + \frac{d\varepsilon_H}{dz} \Delta t \\ z(t+1) &= z(t) + R_z \sqrt{2\varepsilon_V \Delta t} + \frac{d\varepsilon_V}{dz} \Delta t \end{aligned} \quad \dots \quad (A6)$$

The hydrodynamic velocity, u_H , the biological velocity, u_L , and the vertical gradient of vertical eddy diffusivity, $\frac{d\varepsilon_V}{dz}$, are all evaluated at the point $\{x(t), y(t), z(t), t\}$, while the vertical eddy diffusivity is evaluated at the point $\{x(t), y(t), z(t) + \frac{1}{2} \frac{d\varepsilon_V}{dz} \Delta t, t\}$. Here, ε_T , the horizontal eddy diffusivity is not assumed to be constant (see below), and $\frac{d\varepsilon_T}{dz}$ is evaluated at the point $\{x(t), y(t) + \frac{1}{2} \frac{d\varepsilon_H}{dz} \Delta t, z(t), t\}$.

The addition of the spatial gradients of diffusivity and the evaluation of the diffusivities at the shifted locations ensure that the more energetic turbulent eddies experienced by fish in regions further away from the near-wall boundary layers move the fish away from the boundary layers. R_y and R_z are uniformly distributed random numbers between -1 and 1. The rationale behind the formulation in System (A6) is that fish experience forcing to their left or right, and towards the free surface or the river bottom according to the local hydrodynamic forces they experience. These are captured by the random perturbation terms in System (A6). In reality, fish also move actively laterally and vertically within the water column (Olivetti et al. 2021; Gross et al. 2021). The net effect of System (A6) is that biological behavior is adopted in the streamwise direction, and passive particle-like behavior is adopted in the lateral and vertical directions. The compromise avoids expensive flow-dependent estimations of lateral and vertical movement at each behavioral timestep. In subsequent versions of the model, this lateral and vertical movement will be represented using random draws from empirical distributions of lateral movement conditional upon the local water velocity experienced by the fish.

The Delta and, accordingly DSM2, contain two types of channels: straight channels and curved channels. Because the curvature of a channel impacts the shape of the profile in that channel, we

represent these two channel types separately in the model. Whether a channel is straight or curved was determined using a statistical estimation procedure described in Appendix B.

For straight channels, the quantities in System (A6) are evaluated from the following theoretical profile expressions (DWR, 1998):

$$\begin{aligned} u_H &= U f_V f_H \\ f_H &= A + B \left(\frac{2y}{W} \right)^2 + C \left(\frac{2y}{W} \right)^4 \\ f_V &= \begin{cases} 1 + \left(\frac{0.1}{\kappa} \right) \left[1 + \ln \left(\frac{z}{H} \right) \right]; \frac{z}{H} \geq 0.01 \\ 0 \quad ; \frac{z}{H} < 0.01 \end{cases} \end{aligned} \quad \dots \text{(A7)}$$

where W and H are the channel width and depth of the cross-section that the fish is in, U is the mean streamwise velocity, $\{A, B, C\}$ are constants specified in the *ePTM v2* configuration file, and $\kappa = 0.41$ is von Karman's constant, and

$$\begin{aligned} \varepsilon_H &= C_T H u^* \\ \varepsilon_V &= \kappa \frac{z}{H} \left(1 - \frac{z}{H} \right) \\ \frac{d\varepsilon_V}{dz} &= \kappa \frac{1}{H} \left(1 - 2 \frac{z}{H} \right) \\ u^* &\approx 0.1U, \end{aligned} \quad \dots \text{(A8)}$$

where $C_T \approx 0.6$ is a constant, and u^* is the friction velocity.

For curved channels, profiles are represented differently. We implemented a curvature-based reparameterization of the flow and mixing profiles in channels. While the velocity profiles we use are obtained from laboratory experiments in prismatic curved channel flows, in the future, we will use velocity profiles obtained from ADCP measurements in the Delta. To specify flow profiles of the streamwise velocity, vertical and lateral eddy diffusivity and their gradients, we use theoretical profiles for straight channels and vertical velocity profiles and mixing coefficients, and lookup tables based on empirical studies (Appendix C) for the lateral velocity profile and mixing coefficients curved channels. In order to represent particle trajectories realistically and balance the requirements of fidelity and performance, we have tuned several model settings. These are described in Appendix D.

A2.2 Routing at channel junctions:

A second important process that determines how salmonids move through the Delta is how animals move into one downstream channel or another at junctions (Gleichauf et al. 2014; Perry et al. 2014; Hance et al. 2020; Romine et al. 2021). Sridharan et al. (2017) demonstrated the importance of correctly representing the movement of simulated fish through channel junctions. In *ePTM v2*, we allow fish to move into downstream channels at junctions depending on their lateral position relative to the critical streakline (Perry et al. 2014), also known as the bifurcating streamline (Fig. A.1; Sridharan et al., 2017).

When a simulated migrant reaches the end of a channel within a sub-timestep, the routing process is invoked, and it is moved into a downstream channel or open water body. Subsequently, the remainder trajectory computation is completed for that sub-timestep in the new channel beginning from a random cross-sectional position in the new channel. If the fish enters an open water body, it waits for a random length of time between zero seconds and one day and then leaves the open water body randomly into a connecting downstream channel. This mechanism ensures that fish move through the system in a manner consistent with the critical streakline hypothesis, while allowing for random lateral and vertical movements to occur within the time taken to move through the junction.

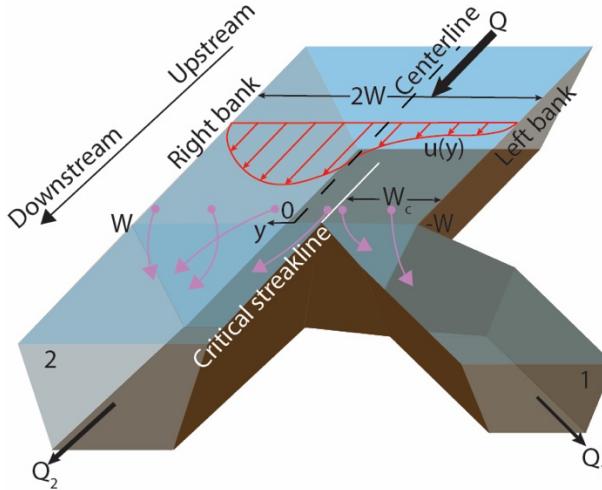


Figure. A.1. Schematic routing of fish (pink dots and arrows) through a channel junction depending on their lateral position relative to the critical streakline (purple line) for inflowing channel.

We compute the position of the critical streakline from the right bank (by convention) as the location till which the flow sums to the flow in the outflowing channel nearest to the left bank.

$$W_c = W \left(\frac{y}{W} \right)_i$$

$$\begin{cases} UHW \sum_{\frac{y}{W}=-1}^{\left(\frac{y}{W} \right)_i} u_i = Q_1; \text{ Inflowing channel directed oceanward} \\ UHW \sum_{\frac{y}{W}=-1}^{\left(\frac{y}{W} \right)_i} u_i = Q_2; \text{ Inflowing channel directed landward} \end{cases} \dots (A9)$$

In the *ePTM v2*, the location of the critical streakline is found by simply dividing the width of the channel by the flow entering one of the downstream channels. We found that integrating the velocity profile to determine where the flow bifurcates does not produce critical streakline locations that are significantly different from estimates produced by using the flow-splits.

When a simulated fish reaches a channel junction, it is assigned to one channel or the other based on its location in the direction normal to the streamwise flow, $y(t)$. Depending on whether $y(t)$ is greater than or less than the location of the critical streakline, W_c , the fish will be assigned to the left channel or the right channel at the junction. The location of the critical streakline is determined as a function of the hydrodynamic parameters, which are fixed or determined through lookup tables to produce as realistic flows as possible as described above. We assume that fish deterministically choose one channel or another based on whether their location in the cross-stream direction is greater than or less than the critical streakline. Thus, the routing module does not contain any fitted free parameters. In the case of junctions with more than three channels, we implemented a tree-search algorithm (Appendix E). We note that it would be straightforward to implement a stochastic routing decision that depends on variables related to the flow, fish position as it reaches the junction, or other modeled features, but we have not implemented this in *ePTM v2*.

A.2.3 Predation and mortality:

Survival in the *ePTM v2* is modeled using a modified version of the *X-T* model developed in Anderson *et al.* (2005). This is a first order rate process in which the probability of surviving through

a given reach decreases with increasing travel time and migration distance. We note that the formulation of the model differs slightly in the *ePTM v2* than that derived in Anderson et al. (2005) due to the representation of the actual path of the fish in our model rather than the definition of survival over a fixed reach length as in the original model. This modification accommodates the nature of how movement paths are simulated in *ePTM v2*.

The objective of the survival model is to express the probability that a migrant survives predation as it moves through a channel that is occupied by predators that are distributed in space. The basic assumptions of the model is that, on average, the risk of encountering and being captured by predators can be expressed as constant per-unit distance and per-unit time rates. This assumption is supported by analyses of fine-scale movements of juvenile Chinook salmon in the San Joaquin River relative to density maps of predator locations, which are also produced from fine-scale acoustic tracking data (Section 3). These analyses suggest that, when averaged over many migrant movements and over the diel cycle, the exposure to regions of high predator density by smolts is similar to that predicted by the long run average of a random walk through the domain (Section 3). Moreover, when moving through a reach, animals that follow longer paths have increased exposure to regions of high predator density.

Our model computes survival probability of each fish in each 15 minute timestep as a function of two quantities: the distance traveled by the fish in the timestep, X , which is computed over movements of fish on the sub-timestep scale of 20 seconds and summed over the 15 minute timestep, and the duration of the timestep, itself. These quantities influence survival probability through the following expression:

$$P(\text{survival}) = e^{-\frac{\sqrt{X^2 + \omega^2 t^2}}{\lambda}}. \quad \dots(A10)$$

Since the dominant timestep is fixed at 15 minutes in the model, $t = \tau = 15$ min. Travel distance, X , however, varies among fish and from one timestep to the next depending on each animal's swimming speed and direction as well as hydrodynamic forcing on the fish. There are two free parameters associated with survival through the system: the parameter, λ , which determines how survival decays with distance traveled through a reach, and the parameter, ω , represents stochasticity in the predator-prey encounters, and with λ , determines how survival probability decays with time (Table A2).

In the standard mode, if a random draw from a uniform distribution is smaller than the probability of survival, fish continue to move through the system. Otherwise, they are killed and the simulation for that fish ends. An alternate mode is also available in the model wherein particles are not removed from the system but rather continue to be simulated. Survival estimates can then be provided for each reach, and compounded over the course of migration, using a fixed population of simulated migrants.

Table A2. *ePTM v2* survival model parameters

Survival component	Description	Fitting parameters
Characteristic length-scale of survival	Determines distance and time-dependence of survival	λ
Time-dependence parameter	Determines time-dependence of survival	ω

A.3 Model fitting and calibration

A.3.1 Calibration data:

In order to make predictions about movement patterns and mortality, free parameters of the *ePTM v2* must be estimated from data. To do this, we used data from tagging studies of late fall run Chinook salmon (2006-2010) released in the Sacramento River and passing through the Delta (Perry 2010; Perry et al. 2010). In total, 1,591 tagged late-fall smolt were released at I-Street Bridge on the Sacramento River and just South of the confluence of the Sacramento River and Georgiana Slough in eight release groups over the five year period (Table A3). These fish were tagged with VEMCO V5 acoustic tags and were tracked through the system at hydroacoustic receiver arrays. By tracking fish through these receiver arrays, their passage through the Delta could be naturally quantified along nine reaches connected by key river junctions (Figure 5.1.1). A Cormack-Jolly-Seber (CJS) mark-recapture model was fit within a hierarchical Bayesian framework to concurrently estimate detection, routing and survival probabilities through the different reaches (Perry 2010; Perry et al. 2018). In addition to the reach-scale survival estimates, the data was also processed to include first detection times for each fish whenever it was detected at a receiver array. This allows us to calibrate the model not only to survival, but also to travel time distributions of fish passage through the system.

We used data from VEMCO-tagged late fall run Chinook (Table A3) to calibrate the model, and more recent JSATS Chinook data as points of independent validation of the model. To validate the model, we selected eleven releases of hatchery-reared JSATS-tagged fall and Winter run fish between 2012 and 2017 of which 1,335 fish made it to the upstream end of the Delta (Table A4).

Table A3. VEMCO-tagged late-fall release calibration dataset details

S. No.	Period	Release Location	Ending Location	Number of fish Released
1	5-6 Dec. 2006	Sacramento	Chippis Island	65
2	17-18 Jan. 2007	Sacramento Discovery Park	Chippis Island	81
3	4-7 Dec. 2007	Sacramento or Georgiana Slough	Chippis Island	209
4	15-18 Jan. 2008	Sacramento Discovery Park or Georgiana Slough	Chippis Island	212
5	30 Nov.-6 Dec. 2008	Sacramento or Georgiana Slough	Chippis Island	293
6	13-19 Jan. 2009	Sacramento or Georgiana Slough	Chippis Island	293
7	2-5 Dec. 2009	Sacramento River at Elk Landing or Georgiana Slough	Chippis Island	233
8	16-19 Dec. 2009	Sacramento River at Elk Landing or Georgiana Slough	Chippis Island	205

Table A4. JSATS-tagged fall and winter-run release validation dataset details

S. No.	Hatchery	Run	Period of Delta entry	First detection location within the Delta	Ending Location	Number of fish at Delta entry
1	Coleman	Fall	24 Apr.-8 May 2012	Tower Bridge	Benicia	18
2	Coleman	Fall	15 Apr.-6 May 2013	Tower Bridge	Benicia	49
3	Coleman	Fall	12 Apr.-10 May 2016	Tower Bridge	Chippis Island	54
4	Coleman	Fall	9 Apr.-6 May 2017	Tower Bridge	Chippis Island	118
5	Nimbus	Fall	15-19 May 2016	Tower Bridge	Chippis Island	220
6	Nimbus	Fall	25 May-4 Jun 2017	Tower Bridge	Chippis Island	204
7	Livingston Stone	Winter	3 Mar.-1 Apr. 2013	Tower Bridge	Benicia	10
8	Livingston Stone	Winter	19 Feb.-23 Mar. 2014	Tower Bridge	Benicia	121
9	Livingston Stone	Winter	9 Feb.-16 Mar. 2015	I80-50 Bridge	Benicia	157
10	Livingston Stone	Winter	22 Feb.-22 Mar. 2016	Tower Bridge	Chippis Island	278
11	Livingston Stone	Winter	10 Mar.-7 Apr. 2017	Tower Bridge	Chippis Island	106

A.3.2 Generating ePTM v2 predictions:

In the ePTM, the model parameters are spatially explicit, in that they can take on different values in different parts of the domain. The rationale behind this design choice is that this allows us to capture changes in behavior at different points along the migration (Section 3). To balance model parsimony with flexibility, we imposed the restriction that parameter values should be constant within each reach. This does not preclude the possibility that some parameters may take on similar values across reaches. In total, *ePTM v2* has eleven free parameters in each of the nine reaches, or 99 model parameters that must be estimated from data. The model parameters were fit to the observed travel time distributions (the distribution of differences between the first detection at the downstream end of the reach and the upstream end of the reach across the observed tagged fish) in each mark-recapture reach, and to the CJS-estimated survival rate through each reach.

To produce predictions from *ePTM v2* for fish in the calibration dataset, we identified the entry time of each fish detected in both the upstream and downstream ends of a reach in the calibration data. For each of these fish, we released 10 simulated migrants in an *ePTM v2* simulation in which hydrologic variables were set to match the conditions at the observation times in the data. The duration of this simulation was set to be ten days longer than the last initial detection time of fish at the downstream end of the reach. For each of the 10 simulated fish corresponding to the single real fish, the fate of the simulated migrant in the reach as well as the travel time through the reach was recorded. This ensemble constitutes a prediction of *ePTM v2* for the observed fish.

Such simulations were carried out independently for each release and reach combination for a given set of parameter values. For each set of parameter values, a total of 72 *ePTM v2* simulations were carried out in which ten replicate fish were simulated for every real fish that traversed the reaches. Particles were initialized at the same locations on the DSM2 grid corresponding to the locations of the telemetry stations demarcating the mark-recapture reaches. By performing such runs over a large set of parameter values, a representation of the model goodness-of-fit to the data was obtained. This was used to estimate model parameters.

A.3.3 Estimating model parameters from data:

The *ePTM v2* model free parameters are shown in Tables A1 and A2. To estimate these parameters from the calibration data, we used the following procedure. First, for each parameter, we identified bounds on the permissible range of parameter values to constrain the parameter search space. These bounds were set based on a thorough review of the literature including laboratory experiments and field data, and reasonable biological expectations when insights could not be gained from the literature.

The mean swimming speed and standard deviation in swimming speed, $\overline{|u_s|}$ and $\sigma_{|u_s|}$, were restricted to a range of 0 to 0.5 m/s based on a survey of the published literature on sustained swimming speeds of Chinook smolts, reported either as the critical swim speed or the maximum swim speed for a wide range of fork lengths (Anglea et al. 2004; Brown et al. 2006; Dougan, n.d., Walker et al. 2016; Lehman et al. 2017). All of these studies report a maximum sustained swimming speed of about 5 body lengths per second (blps). Based on the fork lengths reported in these studies, we assumed an average fork length of approximately 100mm, which produces a maximum value of this parameter of 0.5 m/s. Setting the maximum $\sigma_{|u_s|}$ to also 0.5 m/s results in more than 95% of the draws rarely exceeding a speed of 10 blps, consistent with the range of maximum reported swimming speeds in this system (Lehmann et al. 2017).

The daytime swimming probability, p_{DS} , was allowed to vary from 0 to 1. For California Central Valley Chinook, Chapman et al. (2013) reported that the proportion of fish detected during the daytime versus the nighttime varied as a function of where they were in the system from 10% to 75%. So, we set our bounds to encompass these fractions.

Holding parameters are more difficult to estimate directly from data. We therefore computed the peak flood phase water velocity modeled in the Delta between 1962 and 2017 using DSM2 and set this value as the lower threshold for holding velocity, u_F . The upper threshold for this was set at 0 m/s, which would indicate a propensity for fish to hold even during slack water. The estimated peak flood velocity was -0.55 m/s. It is reasonable to expect that not every fish would hold at all times during opposing flow, but the holding probability, p_H , could not be directly estimated. We therefore allowed it to vary between 0 and 1. For the parameters that determine the shape of the generalized logistic function used to estimate the probability of orienting with the flow at a given timestep, there are no analogues in the literature. We therefore allowed p_M , the probability of memory persistence, and p_{System} , to vary between 0 and 1. A value of $p_{System} > 0.5$ indicates that fish tend to swim with the flow, whereas a value less than 0.5 allows for the possibility that fish tend to swim against the flow. The values of c and β , respectively the half-saturation point and slope of the logistic function of normalized water velocity of the probability of swimming with the flow were bound between -10 and 10, and 0 and 10, respectively. We set these ranges to allow this curve to take on a variety of shapes from linear growth to exponentially saturating within 95% of the range of DSM2-modeled water velocities within the Delta between 1962 and 2017.

The survival parameters, the characteristic length scale and the time dependence parameter, were allowed to vary between 10 and 1000 Km, and 0 and 2 m/s respectively. These bounds were estimated as follows. Perry et al. (2018) showed that survival varies as a function of flow within the

mark-recapture reaches in the Delta. A “*toy PTM*” simulation which involved a very fast random walk of simulated fish with behaviors identical to the ePTM over three reaches representing the Delta in a coarse manner (Appendix F) was carried out in which these parameters were allowed to vary over a range of values that produced aggregated survival estimates spanning the range of values reported in the mark-recapture estimates in Perry et al. (2018). The range of these values was then used to bracket the survival parameters in the *ePTM v2* calibration.

We applied a four-stage calibration process. First, we deduced that the movement parameters could be fit independently of the survival parameters (see below). Second, we performed a coarse grid search on a large number of movement parameter values to narrow in on the best local optima defined within a multiobjective optimization framework. Third, we zoomed into the parameter space in the neighborhoods of the best local optima to perform a fine grid search using the multiobjective optimization framework to identify the global optimum movement parameter values. Fourth, we held the movement parameters at their optimum values and performed a grid search over the survival parameters to find the optimum values these parameters.

The following programming languages were used in the fitting process:

- (i) R v.4.0 to select candidate design parameter value sets and to perform the *toy PTM* simulations (R Core Team 2020).
- (ii) Python v. 3.7 to drive the *ePTM v2* simulations (Python Software Foundation)
- (iii) Matlab v. 2020a to perform the four-stage optimization process (The MathWorks Inc. 2020).

We generated 5,000 design points by sampling a standardized value of each parameter (subtracted the mean of the parameter range and divided by its range) from within the permissible range of values for that parameter using a maximum separation criterion-based space filling algorithm using the R package DiceDesign (Dupuy et al. 2015). For an eleven parameter model for each reach, space-filling algorithms provide an efficient way of sampling significantly fewer points that span the multi-dimensional space more fully than a random selection of points which could fall on lower-dimensional manifolds. To select the optimal space-filling algorithm, we compared ten space-filling algorithms using the R package DiceEval (Dupuy et al. 2015). Using the maximum separation method with a minimum separation criterion of 0.244 produced the best performance of all the approaches across the four metrics (Appendix G). This yielded 5,000 unique parameter sets that could then be used to create model predictions in an independent manner for each reach with whatever the parameter prior expectation ranges are. The calibration dataset contained eight release groups and survival and travel times could be computed reliably from these data for nine of those reaches. This yielded a total of 360,000 *ePTM v2* model runs.

As mark-recapture analysis was used for each reach, we could fit the eleven model parameters for each reach independently of the other reaches. But within each reach, to further reduce the complexity of fitting the 11-dimensional parameter set, we used the *toy PTM* model to identify whether any parameter simplification or decoupling was possible. To do this, we applied the Morris method of elementary effects analysis (Loos and Lemaitre 2014) using the global optimization toolbox developed by Pianosi and Wagener (2015) with the *toy PTM* to study the relationships between the model parameters and the distribution of travel times through the three reaches, and the survival rates in the three reaches. We used the Morris method is an efficient algorithm to study parameter interactions for high-dimensional models. It starts at a random design point of model parameters and cycles through design points by perturbing the value of each parameter a set number of times while holding the values of the other parameters fixed, until all the parameter values are perturbed for the set number of times. This process is repeated for a number of trajectories beginning at a predetermined number of random starting parameter value combinations. So, for 33 parameters in the three-reach *toy PTM*, we began at a 100 randomly chosen parameter value sets within the bounds described above and simulated 3,400 *toy PTM* model runs. In each run,

ten fish were release every two hours over 13 days for a total of 1,560 fish and the simulation was carried out for three simulated months.

To evaluate the travel time distributions through the reaches, we used the Kullbeck-Leibler (KL) divergence between the observed and modeled travel times in each reach. To evaluate the survivals through the reaches, we used the absolute difference between modeled and CJS-predicted survivals. The Morris method allows us to simultaneously evaluate the importance of each parameter and its two-way interaction with every other parameter as follows. If the mean of the gradient in the goodness-of-fit measure (the KL divergence in travel time distributions or the absolute difference in survivals) with respect to a parameter (called the elementary effect) over all the trajectories is small, then this parameter is unimportant on its own. If it is large, then it is important on its own. If the standard deviation in the elementary effect over all the trajectories is small, i.e., the gradient with respect to this parameter does not change by much when the other parameters change, then this parameter does not interact with other parameters. If the standard deviation in the elementary effect over all the trajectories is large, then this parameter likely interacts with other parameters. By performing this analysis with the *toy PTM*, we discovered that for simulating travel times, the survival parameters do not matter, while for simulating survival, the movement parameters are not very important (Figure A.2). We subsequently decoupled the model fitting process for the full ePTM to first fit the nine movement parameters, and then fit the two survival parameters holding the movement parameters at their optimal values.

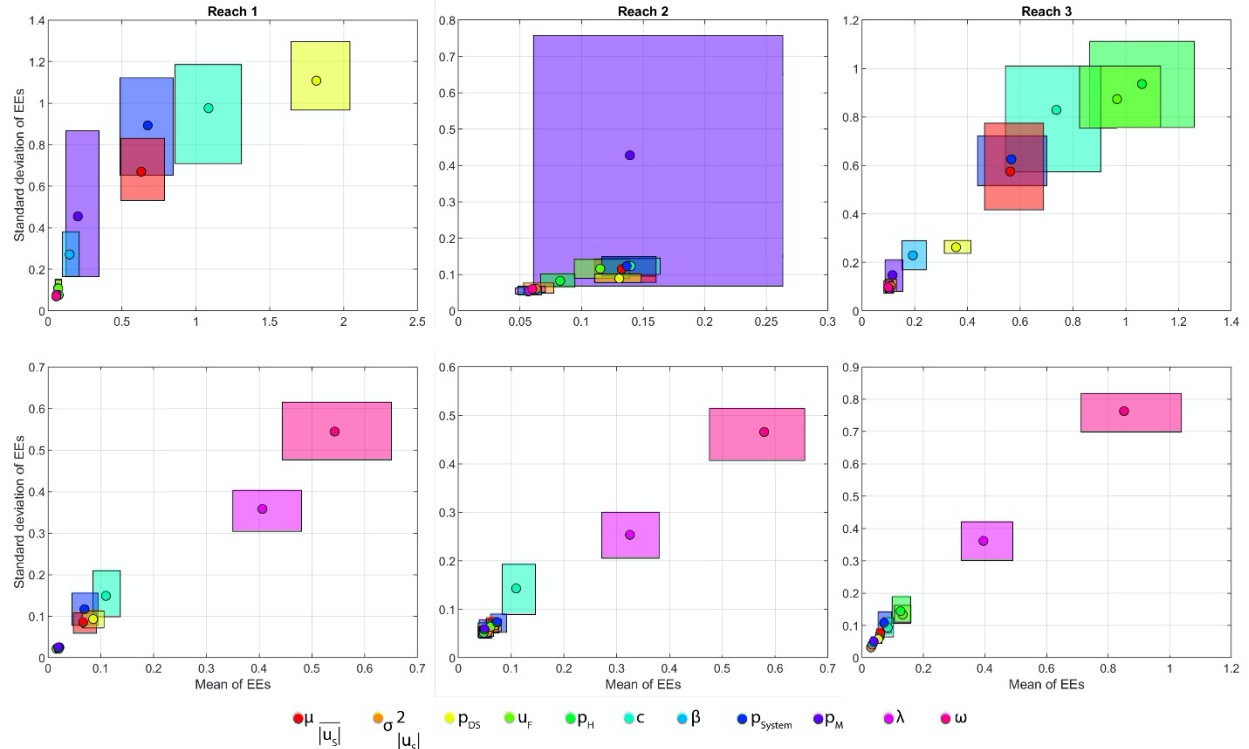


Figure A.2. Elementary effects analysis for the three *toy PTM* reaches. Top row indicates the elementary effects with respect to the KL divergence between modeled and observed travel time distributions and bottom row indicates the elementary effects with respect to the absolute difference in modeled and CJS-predicted survival rates as the goodness-of-fit measures. Each circle and the box around it respectively indicate the mean of the absolute value of pointwise gradient of the goodness-of-fit measure with respect to a parameter on the X-axis and the standard deviation of the pointwise gradient of KL-divergence with respect to that parameter on the Y-axis marginalized over all the other parameter values, and bootstrapped confidence bounds about the means and standard deviations. Colors corresponding to the parameters are indicated in the legend. Elementary effects close to zero on both axes indicate that a parameter is unimportant. The goodness-of-fit surface with respect to this parameter and any other parameter looks like a plane. Large mean and small standard deviation values indicate that a parameter is important

by itself, i.e., the gradient with respect to this parameter changes when its value changes, but is relatively insensitive to changes in values of other parameters. The goodness-of-fit surface with respect to this parameter and any other parameter looks like a function extruded along the axis of the other parameter. Large standard deviation and small mean values indicate that a parameter is not important by itself, but only becomes important when it interacts with other parameters, i.e., the gradient with respect to this parameter changes only when some other parameters' values change. The goodness-of-fit surface with respect to this parameter and any other parameter looks like a function extruded along the axis of this parameter. Large mean and standard deviation values indicate that a parameter is important both by itself and in interactions with other parameters. The goodness-of-fit surface with respect to this parameter and some other parameter has a generally convex shape.

To identify the movement parameter set that produced predictions that best aligned with data, we used several methods for evaluating model goodness-of-fit in a two-stage multiobjective optimization framework. The two-stage framework was necessary because the goodness-of-fit surfaces contain many local optima. To fit all parameters aside from the survival parameters, we focused on goodness-of-fit measures that compare predicted and observed travel times using three goodness-of-fit measures. These were the earthmover's distance between observed and modeled travel times (Levina 2001), the log likelihood of observed travel times conditional on *ePTM v2* parameters (Appendix H), and the intersection over union of the observed and predicted travel time distributions, or the Jaccard index (Chung et al. 2019). The choice of these measures allowed us to evaluate goodness-of-fit from three perspectives: information theoretic with the earthmover's distance, maximum likelihood and visual comparison with the Jaccard index. For each reach in the dataset, we defined the overall goodness of fit by the sum of the goodness-of-fit measure over all release groups observed in that reach. While this results in an exact mathematic value for the log-likelihood, it is only approximately correct in the case of the earthmover's distance and the Jaccard Index. To calculate the earthmover's distance, we used the toolbox developed by Yilmaz (2021). In the three-dimensional space of the three goodness-of-fit measures, we identified the top 10 % of design points along the Pareto front of performance and select the top 10 of these design points. This Pareto front is the set of design points with the lowest negative log-likelihood, the maximum Jaccard index and the minimum earthmover's distance summed over all releases. Given the highly nonlinear interaction of the parameters in a high-dimensional space, it is difficult to visualize this Pareto front.

After identifying these candidate optima, we then performed a second step in which we selected 500 new design points each in the vicinity of candidate optima using the maximum separation space-filling approach as before to obtain a revised candidate set of 5,000 design points. We then repeated the multiobjective analysis as before to identify the top 10% of design points along the new Pareto front within the neighborhoods of the optima from the first iteration. The top performing set of parameter values as defined by the earthmover's index was then chosen as the global optimum for each reach. We chose to use the earthmover's distance for selecting the global optima rather than a combination of the three goodness-of-fit measures because there is no guarantee that the best goodness-of-fit across all three measures will be obtained by any single set of parameter values. We also note that in most reaches, there were fewer than 100 fish in the analysis. So, under such data-limited circumstances, an empirical goodness-of-fit measure such as the earthmover's distance is more robust than a theoretical measure like the log-likelihood. This also influenced our final choice.

We note that except in the case of the standard deviation in swimming speed, the holding threshold, the daytime swimming probability, and the characteristic survival length scale, the spread in the top twenty best performing parameter sets on the Pareto front was very tight. These parameters are difficult to constrain as well as estimate from the data. In the case of the other parameters, the widest spread in the top performing parameter sets on the Pareto front was observed in reach 6 for the half-saturation point on the logistic orientation function and the probability of memory persistence, where the flow is strong, but regularly reverses. So it is not unreasonable that the

parameters associated with the swimming orientation should be sensitive to the timing of fish releases in this reach. We note here that there is no guarantee that the set we have identified using this two-stage approach is indeed the global optimum, but we are fairly confident that it is close to the true global optimum.

To fit the two parameters related to survival, λ and ω , we used optimal values of all the other parameters determined by the method described above, and selected 625 design points, each defined by a pair of values for λ and ω . The goodness-of-fit measure for this optimization step was defined as the sum of the absolute differences between modeled and CJS-predicted survivals for all the releases within a reach. For each design point, we computed survival in each reach by running the model as described in Section 3.2 above. The goodness-of-fit surface for the λ and ω parameters is well behaved and has a well-resolved peak, so that a multistage optimization approach as before is not necessary.

A.4 Results of Calibration and out-of-sample testing

Results of the *ePTM v2*, show strong agreement with many of the major patterns evident in Chinook acoustic telemetry data. Moreover, parameter estimates reflect the behavioral patterns evident in our purely empirical analyses of data in Section 3 of this report. These agreements between model and data suggest that (1) *ePTM v2* is capable of capturing the salient features of salmonid migration through the Delta to make accurate predictions, and (2) the module structures, assumptions, and interpretation of parameters are consistent with empirically observed behaviors of out-migrating fish in the system.

Reach-dependent survival estimates are shown in Figure 5.1.2. Predicted survival by *ePTM v2* shows strong agreement with data in reaches spanning the Delta. In general, predicted survival estimates are within ± 0.2 of observed survivals throughout the Delta, indicating that the model is able to capture patterns of survival and mortality across the diverse habitat and hydrologic conditions present in different regions of the Delta.

A second variable that can be predicted by *ePTM v2* is the distribution of migrant travel times in reaches throughout the system. Acoustic telemetry data yields detections at upstream and downstream stations of a given reach and these detections can be used to compute empirical travel times for all fish detected at both stations. *ePTM v2* can generate travel time predictions for the same fish by initializing simulated migrants at the upstream reach at times that are matched to observed arrival times and then simulating movement of migrants until they arrive at the location of the downstream station. Figure 5.1.3 shows predicted and observed travel time distributions, represented as the cumulative distribution function of observed (black) or predicted (red) travel times through the reach for different reach by release group combinations. The model predictions show strong agreement with travel time distributions for nearly all release by reach combinations. This confirms that the model is able to simultaneously capture survival dynamics and movement dynamics through the Delta.

Parameter estimates for the optimal values of the 11 model parameters are shown for each Delta reach (as defined in our analysis) in Figure A.3. For the active swimming component of the model, large values of the mean swimming speed, \bar{u}_S , combined with small values of the probability of rheotaxis, p_{System} , and a strong probability of memory persistence, p_M , in the north Delta reaches result in fish actively swimming against strong riverine flows. In the more tidally reversing central, south and western Delta regions, decreasing mean swimming speeds, probabilities of rheotaxis typically exceeding 0.5 and reduced memory persistence result in fish executing either movements that are directed weakly with or against the flow. The standard deviation in swimming speeds, $\sigma_{|u_S|}^2$, generally increases through the Delta. Together, these parameters result in actions by

the fish that increase migration rate and increasing dispersion with increasing proximity to the ocean, as we observed in the acoustic telemetry datasets (Fig. 3.2.2)

The orientation and holding parameters allow simulated fish to exhibit different swimming behaviors over the tidal cycle (e.g., Fig. 3.2.3). The trends in the half-saturation point, c , and slope, β , of the logistic orientation probability function are both decreasing from the upstream end to the downstream end of the Delta. In the riverine reaches with strong oceanward flows, the net effect of these parameters in combination with the small values of p_{System} is to orient fish against the flow much more often than with the flow. In the tidal regions, these parameters allow the logistic response to be small when flows are weak, and thereby result in fish orientations that may switch between with and against the flow. When the tide is ebbing and flows are directly strongly oceanward, the combination of these parameters and p_{System} allows fish to be oriented more often with the flow. During strongly landward flow reversals, the threshold holding velocity, u_F , and values of the holding probability, $p_H > 0.5$, result in fish approximately maintaining position. The probability of swimming during the day, p_{DS} , is around 0.5, with no appreciable trend through the system, which is consistent with the values of around 0.34 to 0.75 obtained in this region from acoustic telemetry experiments by Chapman et al. (2013).

The characteristic length scale, λ , generally increases downstream through the system, while the time-dependent survival parameter, ω , generally decreases. This results in an overall increasing likelihood of survival through the downstream reaches of the system.

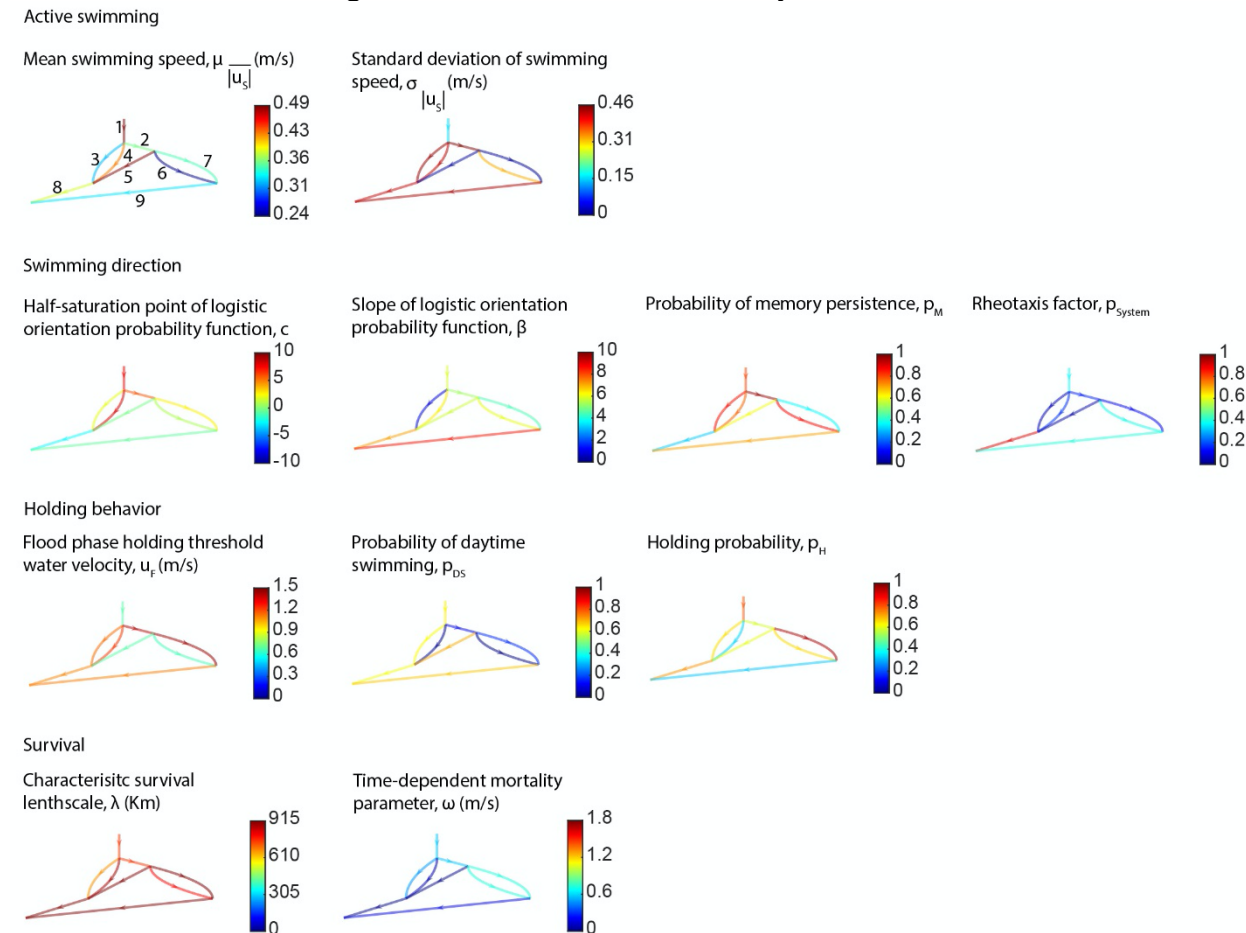


Figure A.3. Parameter estimates across Delta reaches. Schematic of Delta reaches with optimal parameter values indicated by color.

A.4.1 out-of-sample testing

To evaluate predictions of the *ePTM v2* using data that were not included in model fitting, we used data from the California enhanced acoustic tagging project, which provides arrival data and CJS survival estimates for different JSATS tagged Chinook runs and water years (<https://oceanview.pfeg.noaa.gov/CalFishTrack/>). We used data that met several criteria: (1) runs of Chinook studied were fall or winter, (2) the release group size at the release site was greater than 100 fish, and (3) the fish were observed at least at the telemetry stations at Sacramento and either at Chipps Island or Benicia. This resulted in 11 run by release group by water year combinations against which to compare *ePTM* predictions. Survival predictions for out-of-sample runs were produced in the same way as the predictions for the training data described above. Results are shown in Figure 5.2.1, which shows observed and predicted survival of Chinook salmon passing through the Delta as a function of mean flow in the Sacramento River. *ePTM v2* predictions capture the major patterns evident in data. Firstly, through-Delta survival predictions of the model (Fig. 5.2.1 red squares) compare favorably with direct estimates from data (Fig. 5.2.1, black circles). In most cases, the survival prediction is within 0.2 of the observed survival, and in some cases it is much closer. Secondly, the model recovered the shape and scale of the observed relationship between survival and mean river flow through the Sacramento during migration through the Delta (Fig. 5.2.1, lines and confidence intervals). Not only are all data used to compute observed survival out-of-sample (i.e. they were not used in the model calibration), none of the data used in model calibration (late fall run Chinook 2006-2010) overlap in time with the out-of-sample data (fall and winter run Chinook 2012-2017). We, therefore, believe this comparison provides a strong test of the performance of *ePTM v2* in forecast mode.

In many cases, CJS survival estimates were reported for the JSATS data at Benicia rather than at Chipps Island. In such cases, we utilized the approach outlined in Appendix I to convert these survivals to survivals that would have been nominally reported at Chipps Island.

Another aspect of out-of-sample validation is model performance in predicting migration routing. To study how the model performs in predicting out-of-sample route use by salmon through the system, we selected those releases of the JSATS program in which fish passages were recorded through two key junctions along the Sacramento River: the Mainstem Sacramento with Sutter and Steamboat Sloughs, and Georgiana Slough. This resulted in a selection of the 2014 and 2015 releases. Results are shown in Figure 5.2.2, which shows observed and predicted salmon detected along different possible routes at the two junctions. To further elucidate the fine-temporal scale of the model, we stratified this comparison by phase of the tide, defined at the junction with Sutter and Steamboat Sloughs with respect to the flow reversal in Steamboat slough, and at the junction at Georgiana Slough with respect to the flow reversal in Georgiana Slough. In both years, the model is able to predict the qualitative patterns in the data correctly, and quantitative routing probabilities to $\pm 20\%$ from the observed values, which is remarkable given that routing was not calibrated in the model. We also note that a fish guidance structure was in place in 2014 at the head of Georgiana Slough with an overall passage efficiency of 0.777 (DWR 2016). This was represented in the model as a particle filter.

A.4.2 Model sensitivity

To evaluate the sensitivity of the model to parameters, we focused on the *toy PTM*, which is a spatially coarsened version of *ePTM v2*. In the future, we will conduct a full sensitivity analysis on *ePTM v2*. However, we note that since the model structure of the two models is identical, and that the flows driving the two models are real flows either simulated or measured in the Delta, with the only difference being the simplification of the *toy PTM*'s model grid. By examining the results of the elementary effects analysis in Figure A.2, along the horizontal axes in that figure, we can deduce

several aspects of the model sensitivity to parameters. In all the regions, the modeled survivals are primarily sensitive only to the survival parameters, λ and ω (lower panels in Figure A.2).

We observe that in the riverine reaches upstream of Georgiana Slough (top left panel in Figure A.2 corresponding to reach 1 in the toy PTM), the modeled travel times are likely most sensitive to the probability of daytime swimming, p_{DS} , the half-saturation point of the logistic orientation probability function, c , the probability of rheotaxis, p_{System} , and the mean swimming speed, $\bar{|u_S|}$ (the parameters with the strongest elementary effects). The model is relatively insensitive to the slope of the logistic function, β , and standard deviation in swimming speed, $\sigma_{|u_S|}^2$, here owing to the strong oceanward currents and low observed spread of fish in this region.

In Georgiana Slough, the Delta Cross Channel and in the interior Delta (top middle panel in Figure A.2 corresponding to reach 2 in the toy PTM), we observe that the probability of memory persistence, p_M , p_{System} , p_{DS} , $\bar{|u_S|}$, $\sigma_{|u_S|}^2$ and β contribute significantly to the sensitivity of the travel time simulation. This is because of the tidal nature of the flows in this region. The sensitivity to β in this region indicates that the shape of the logistic function, which dictates the rapidity of the response to changing flows is important here. Low values of β will result in the probability of orienting with the flow responding sluggishly to changing flows, while large values will ensure a more rapid response.

In the Southwestern reaches of the Mainstem Sacramento River (top right panel in Figure A.2 corresponding to reach 2 in the toy PTM), the travel time simulations are most sensitive to the holding threshold water velocity, u_F , probability of holding, p_H , c , $\bar{|u_S|}$ and p_{System} . In this region, the dispersion of fish in the acoustic tagging data is large, and therefore the model is insensitive to values of $\sigma_{|u_S|}^2$. However, as the flow strongly reverses here, fish behaviors will be highly sensitive to assumptions about the holding and rheotaxis mechanisms and these parameters will determine whether the model is able to recover the observed tidal ratcheting.

The expectation of a well-constructed mechanistic model is that any sensitivity analysis should reveal parameter dependencies that will functionally change behavioral responses depending on the nature of the causal relationships hypothesized by the values of the most important parameters in the model. In a spatially explicit model such as the ePTM, the relative importance of parameters can vary spatially as the mechanisms underlying the physical movement of fish changes. The sensitivity analysis done using the toy PTM is able to qualitatively confirm that the model is able to represent the hypothesized mechanisms of fish movement outlined in this Appendix.

References

- Blanckaert, K., & De Vriend, H. J. (2004). Secondary flow in sharp open-channel bends. *Journal of Fluid Mechanics*, 498, 353-380.
- Chernov, N. (2010). Circular and linear regression: Fitting circles and lines by least squares. CRC Press.
- Chung, N. C., Miasojedow, B., Startek, M., & Gambin, A. (2019). Jaccard/Tanimoto similarity test and estimation methods for biological presence-absence data. *BMC bioinformatics*, 20(15), 1-11. <https://doi.org/10.1186/s12859-019-3118-5>.
- Dupuy, D., Helbert, C., & Franco, J. (2015). DiceDesign and DiceEval: Two R packages for design and analysis of computer experiments. *Journal of Statistical Software*, 65(11). 10.18637/jss.v065.i11.
- Gandhi, B. K., Verma, H. K., & Abraham, B. (2016). Mathematical modeling and simulation of flow velocity profile for rectangular open channels. *ISH Journal of Hydraulic Engineering*, 22(2), 193-203.
- Gilbert, Richard O. (1987), "6.5 Sen's Nonparametric Estimator of Slope", *Statistical Methods for Environmental Pollution Monitoring*, John Wiley and Sons, pp. 217–219, ISBN 978-0-471-28878-7.

- Glechauf, K. T., Wolfram, P. J., Monsen, N. E., Fringer, O. B., & Monismith, S. G. (2014). Dispersion mechanisms of a tidal river junction in the Sacramento–San Joaquin Delta, California. *San Francisco Estuary and Watershed Science*, 12(LA-UR-14-29557).
- Levina, E., & Bickel, P. (2001, July). The earth mover's distance is the mallows distance: Some insights from statistics. In *Proceedings Eighth IEEE International Conference on Computer Vision. ICCV 2001* (Vol. 2, pp. 251-256). IEEE. [10.1109/ICCV.2001.937632](https://doi.org/10.1109/ICCV.2001.937632).
- Liao, J. C. (2007). A review of fish swimming mechanics and behaviour in altered flows. *Philosophical Transactions of the Royal Society B: Biological Sciences*, 362(1487), 1973-1993.
- Michel, C. J., Henderson, M. J., Loomis, C. M., Smith, J. M., Demetras, N. J., Iglesias, I. S., ... & Huff, D. D. (2020). Fish predation on a landscape scale. *Ecosphere*, 11(6), e03168. <https://doi.org/10.1002/ecs2.3168>
- Miles, J., Vowles, A. S., & Kemp, P. S. (2021). The response of common minnows, *Phoxinus phoxinus*, to visual cues under flowing and static water conditions. *Animal Behaviour*, 179, 289-296.
- Notch, J., R. Robinson, T. Pham, R. Logston, A. McHuron, A. Ammann, C. Michel. 2021. Enhanced Acoustic Tagging, Analysis, and Real-Time Monitoring of Wild and Hatchery Salmonids in the Sacramento River Valley – 2018 - 2020 Final Report. Report prepared by University of California – Santa Cruz for the U.S. Bureau of Reclamation under contract USDI/BOR# R18AC00039.
- Oteiza, P., Odstrcil, I., Lauder, G., Portugues, R., & Engert, F. (2017). A novel mechanism for mechanosensory-based rheotaxis in larval zebrafish. *Nature*, 547(7664), 445-448.
- Perry, R. W., Pope, A. C., Romine, J. G., Brandes, P. L., Burau, J. R., Blake, A. R., ... & Michel, C. J. (2018). Flow-mediated effects on travel time, routing, and survival of juvenile Chinook salmon in a spatially complex, tidally forced river delta. *Canadian Journal of Fisheries and Aquatic Sciences*, 75(11), 1886-1901. <https://doi.org/10.1139/cjfas-2017-0310>
- Pianosi, F., & Wagener, T. (2015). A simple and efficient method for global sensitivity analysis based on cumulative distribution functions. *Environmental Modelling & Software*, 67, 1-11. <https://doi.org/10.1016/j.envsoft.2015.01.004>.
- Python Software Foundation. Python Language Reference, version 2.7. Available at <http://www.python.org>.
- R Core Team (2020). R: A language and environment for statistical computing. R Foundation for Statistical Computing, Vienna, Austria. URL <https://www.R-project.org/>
- Romine, J. G., Perry, R. W., Stumpner, P. R., Blake, A. R., & Burau, J. R. (2021). Effects of Tidally Varying River Flow on Entrainment of Juvenile Salmon into Sutter and Steamboat Sloughs. *San Francisco Estuary and Watershed Science*, 19(2).
- Ross, O. N., & Sharples, J. (2004). Recipe for 1-D Lagrangian particle tracking models in space-varying diffusivity. *Limnology and Oceanography: Methods*, 2(9), 289-302.
- The MathWorks Inc. (2020). MATLAB. version R2020a. Natick, Massachusetts:
- Visser, A. W. (1997). Using random walk models to simulate the vertical distribution of particles in a turbulent water column. *Marine Ecology Progress Series*, 158, 275-281.

Appendix B. Determining channel curvature

To determine which profiles to use in each channel in *DSM2*, we performed a statistical procedure to determine which channels are actually straight, and which are curved. For a densely up-sampled set of points from the GPS coordinates of the centerpoint of each cross-section used in a *DSM2* channel from the *CSDP* program, we fit both a Theil-Sen robust Linear Regressor (LR) [Gilbert, 1987], as well as a Chernov-Lesort robust Circular Regressor [CR] (Chernov, 2010). If the R² value of the LR exceeded that of the CR, or if the CR estimated a Radius of Curvature (ROC) exceeding 10,000Km, we considered the channel to be straight. Otherwise, the channel was considered to be curved with the *ROC* value estimated by the CR (Fig. B.1). We then determined the angle of the channel bend as

$$\theta = \frac{L}{ROC}$$

$$L = \sum_{i=2}^n \sqrt{(E_i - E_{i-1})^2 + (N_i - N_{i-1})^2} \quad \dots (B1)$$

for n points each with UTM Easting and Northing given by $\{E_i, N_i\}$. We note that in this approach, meandering channels can be represented only as an effective curvature, with the compromise that flow velocity distributions over small-scale meanders will adjust over the large scale channel morphology.

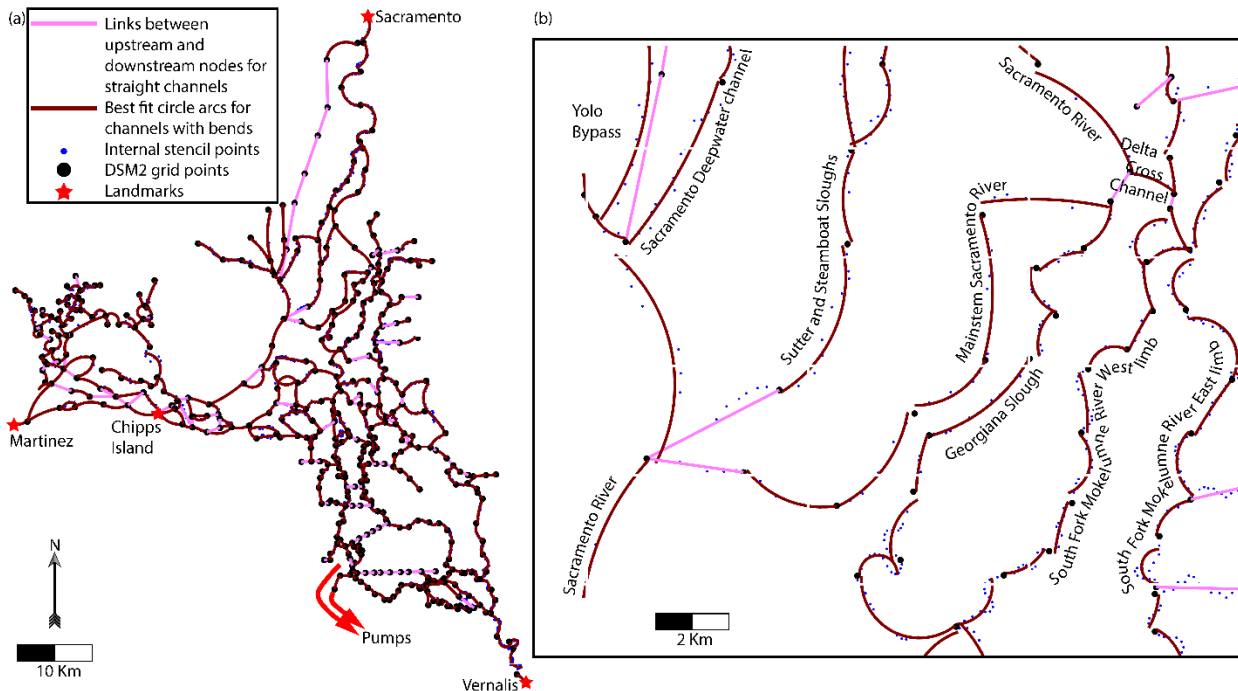


Figure B.1. Channels of DSM2 that are either straight or curved: (a) the whole grid and, (b) zoomed in to the Georgiana Slough region to demonstrate the curve-fitting process.

For each channel, we assign an orientation flag of 1 (directed oceanward) or -1 (directed landward), a bend flag of 0 (straight) or 1 (curved), and a bend direction flag (Figure B.2) of -1 (counter-clockwise), 0 (straight), or 1 (clockwise).

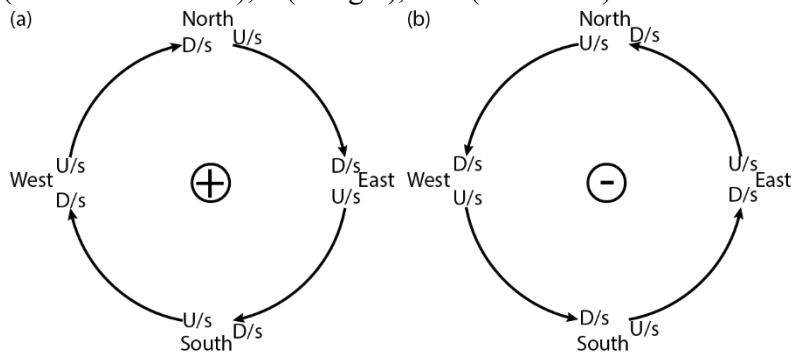


Figure B.2. Bend orientation for curved channels: (a) clockwise, and (b) counter-clockwise.

Appendix C. Developing flow profile lookup table for curved channels

To accurately represent flow profiles in curved channels within the Delta, we developed a lookup table based on previously published empirical results. In particular, we use the experimental results of Gandhi et al. (2016) of turbulent open rectangular channel flow in around bends of varying curvature from a straight channel to up to 90°. For angles beyond 90°, we assume that the flow adjustment will not be significantly different (Blancaert and De Vriend, 2004), and so we use the distribution at 90° itself. We use the best-fit regression of Gandhi et al. (2016) to their data to generate the flow profiles shown in C.1.

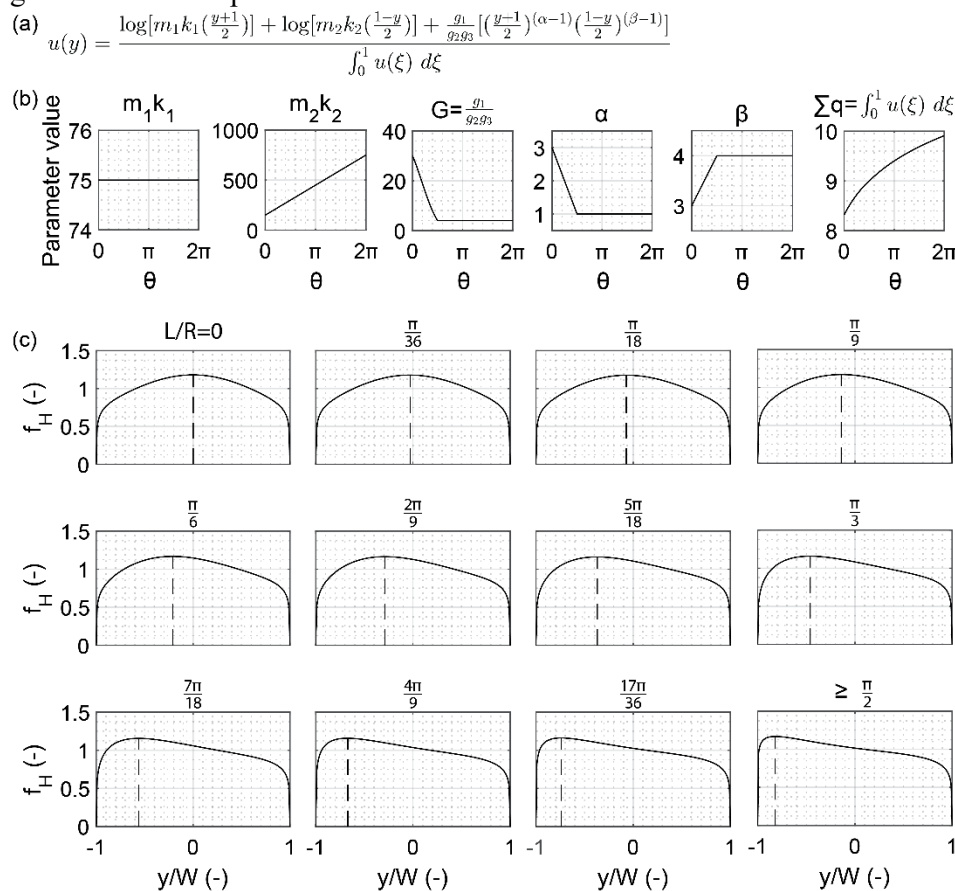


Figure C.1. Lateral profiles of the streamwise velocity obtained by Gandhi et al. (2016) in flume experiments: (a) best fit model reported in Gandhi et al. (2016), (b) fitted parameter values as a function of bend angle, and (c) normalized velocity profiles for various bend angles.

Using the force balance between the turbulent eddy diffusivity and the shear stress by assuming a linear decay of the shear stress from its peak value at the channel banks to zero at the lateral position of peak flow defined from the left bank, y_{Max} (and similarly for the right bank),

$$\varepsilon_H \frac{du}{dy} = u^{*2} \left(1 - \frac{y}{y_{Max}} \right) \quad \dots (C1)$$

where $\frac{du}{dy}$ is obtained from the data, and smoothing the resulting profile of ε_H to remove spurious discontinuities, we get profiles of the flow and mixing terms as shown in Figure C.2.

We generated lookup tables with 1,000-point (rows) lateral profiles with normalized coordinates $\frac{y}{W}$ for the normalized velocity and mixing terms for channel bend angles from 0 to 360° in increments of 17.6715° (columns) for the clockwise curved channels in which the left bank is the outer bank.

Lookup tables for the counter-clockwise curved channels can be generated by inverting the rows of the clockwise lookup tables.

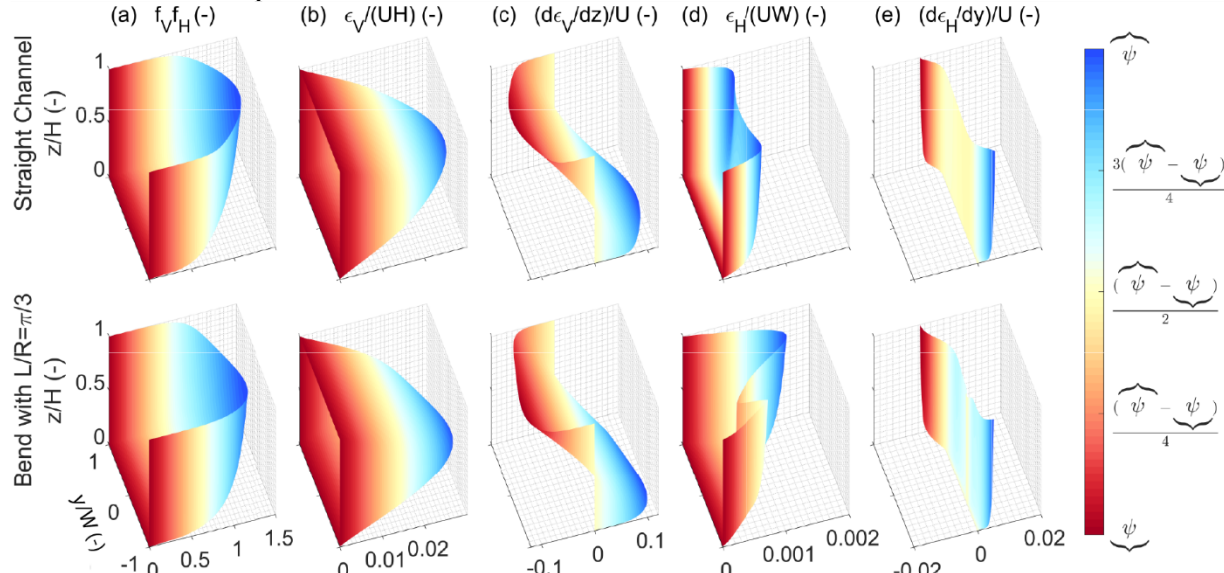


Figure C.2. Profiles for a straight channel and a 60° bend: (a) streamwise velocity, (b) vertical eddy diffusivity, (c) vertical gradient of vertical eddy diffusivity, (d) lateral eddy diffusivity, and (e) lateral gradient of lateral eddy diffusivity.

Appendix D: Model tuning

Per the recommendations in Ross and Sharples (2004), we implemented a mixed layer near the channel banks to eliminate the problem of profile discontinuity. In order to ensure that the ePTM v2 is able to scale as a performance code, we tested a variety of mixed-layer thicknesses to eliminate the problem of vanishingly small timesteps associated with stability constraints in this approach. Based on this analysis, we found that a near-bank and near channel bottom and free surface mixed layer thickness of 20% of the channel width produces only almost 10% deviation from a uniformly well-mixed concentration profile for passive particles initially well mixed laterally. As the mixed layer thickness exceeds 20%, any advantages of using lateral mixing profiles diminish towards using a uniform diffusion coefficient, which produces no lateral variability in density of fish.

Finally, the previously implemented particle tracking module in DSM2 (PTM) has a default timestep of 15 minutes. In order to ensure numerical stability as well as performance for large multi-year simulations, we tested a variety of alternative timesteps. We used a metric of the moment arm of deviation from uniform, or the absolute value of the deviation of the location of the center of mass from the channel center of an initially uniformly distributed mass of passive particles after two days. We found that a timestep of 20s produces an optimal tradeoff between runtimes and model consistency. Thus, the current version of the *ePTM v2* has a primary timestep of 15 minutes, but a sub-timestep of 20s, wherein, particle trajectory computations are carried out over 20s intervals within each primary timestep.

Appendix E: Routing model for complex junctions

In *DSM2*, there are several junctions with more than 3 channels (Figures E.1, E.2). We therefore broke such junctions into a cascade of three-channel sub-junctions, and added zero-length temporary channels to each sub-junction. We assigned these temporary channels such that the flow and head gradient requirements would be met at each junction. This resulted in a tree-search algorithm, wherein the junction cascade is constructed dynamically as a tree originating at the channel the particle is currently in, and we decide which way a particle should go depending on its position relative to the critical streakline.

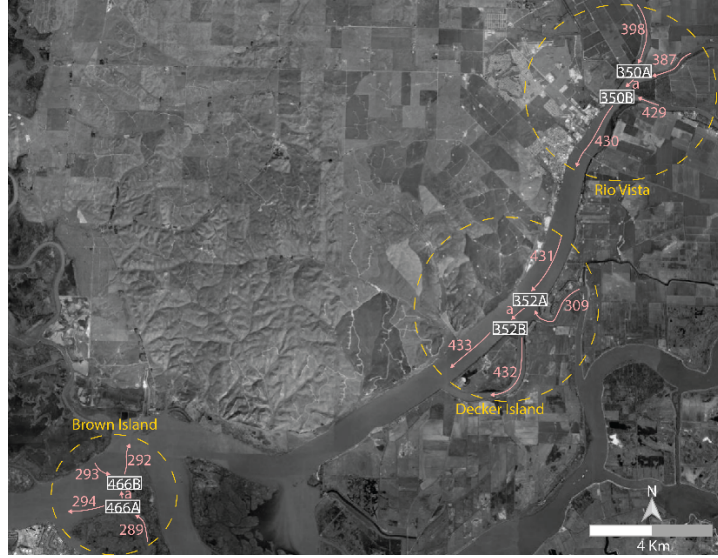


Figure E.1. X-configuration junctions on the Sacramento River (dashed yellow circles), channels (pink arrows), temporary channels (alphabetized) and sub-junctions (Boxed numbers).

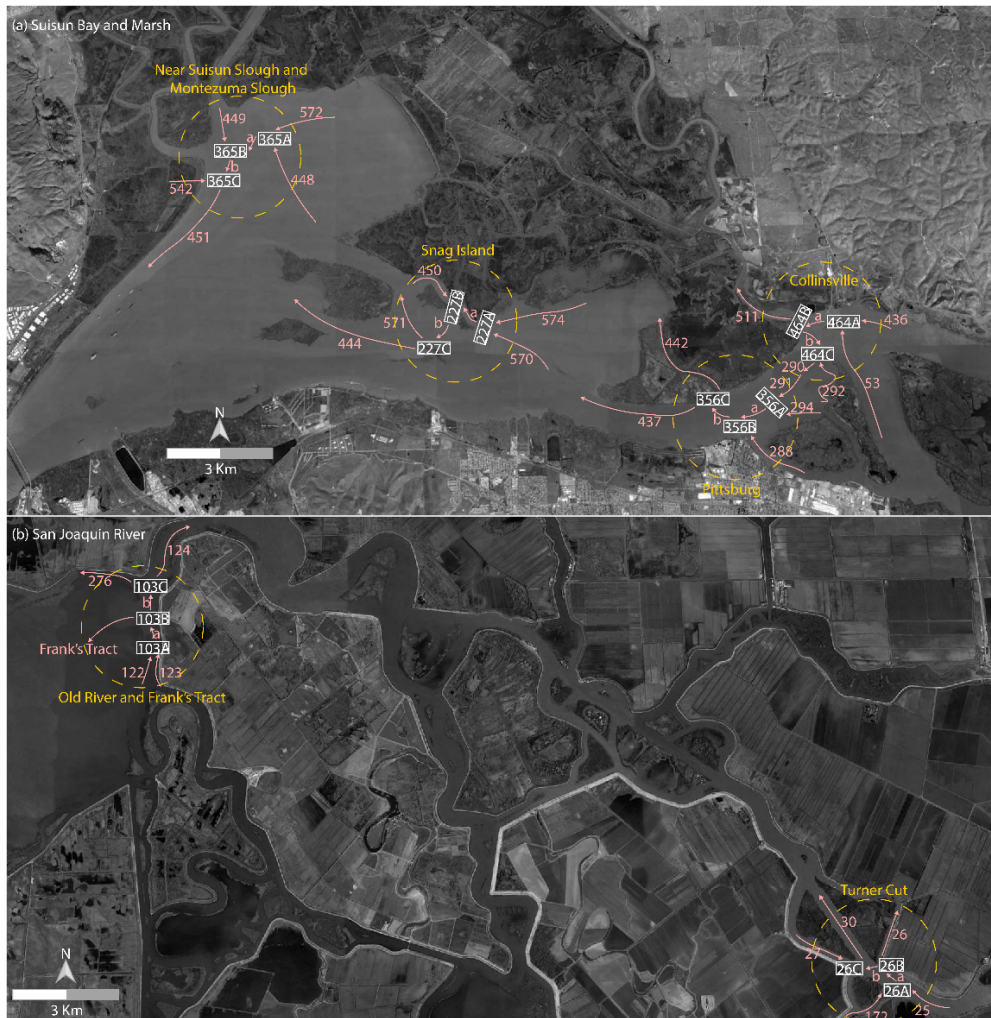


Figure E2. 5-channel junctions (a) in Suisun Bay, and (b) on the San Joaquin River.

This algorithm is most readily understood with the help of an example. The pseudo-code for the junction rule is shown in Figure E3.

Pre-processing:	Read in Junctions.csv (see sample below):			
Node	C1	C2	C3	
339	418	-419	-379	Y-configuration junction
350	398	387	-35000	X-configuration junction with two sub-junctions and temporary channel number CNx1000
35000	35000	429	-430	5-channel junction with three sub-junctions and temporary channels numbered CNx1000 and CNx1000+1
356	291	294	-35600	
35600	35600	288	-35601	
35601	35601	-437	-442	

In this table, all the channels connected to the node are listed clockwise. This table contains all the junctions and Y-configuration sub-junctions in the DSM2 grid. Negative CNs indicate that the upstream end of the channel is connected to the junction, and positive CNs indicate that the downstream end of the channel is connected to the junction. For sub-junctions, the junction number is multiplied by 1000, and then incremented by 1 as required.

- Step 1: Compute the current position of the fish, $\{x(t), y(t), z(t)\}$ from its previous position, $\{x(t-1), y(t-1), z(t-1)\}$ using the algorithm in Figure 5. If $x(t) > L$ or $x(t) < 0$, then compute $x_F = x(t) - L$ or $x_F = -x(t)$ respectively, and $\Delta t_F = \Delta t - \frac{x_F}{u(x,y,z,t-1)}$, then move fish to the end of the channel with a time step of $\Delta t - \Delta t_F$ using the algorithm in Figure 5, and finally assign its current position $\{x(t_{1-F}), y(t_{1-F}), z(t_{1-F})\}$.
- Step 2: Get current position of the simulated fish, $\{x(t), y(t), z(t)\}$, DSM2 channel number and half-width, $W(x)$, and depth, $H(x, t)$, of the cross-section the fish is occupying. Store a flag value of -1 or 1 respectively if the fish is occupying the upstream or downstream end of the channel.
- Step 3: Compute $u(x, y, z, t)$ using steps 1 to 3 in the algorithm in Figure 5.
- Step 4: If the flag value is 1, then compute W_c using the second expression in equation (7).
Else, compute W_c using the first expression in equation (7).
- Step 5: Get the node number of this junction by finding the row in the lookup table above in which $\text{flag} \times \text{CN}$ is present. From this row, get the channels connected to this junction. Depending on which column the current channel is at, label the channels in the columns to its right cyclically as 1 and 2 respectively.
- Step 6: If in the lookup table row, (CN is positive & $y(t_{1-F}) \geq W_c$) | (CN is negative & $y(t_{1-F}) \leq W_c$) then the fish is assigned to the channel labeled 2 and the label of the new channel is stored.
Else if in the lookup table row, (CN is positive & $y(t_{1-F}) < W_c$) | (CN is negative & $y(t_{1-F}) > W_c$) then the fish is assigned to the channel labeled 1 and the label of the new channel is stored.
- Step 7: If the fish enters a $\text{CN} > 1000$, which is a temporary channel, then, assign a flag value of 1, repeat step 5, subsequently assign the new channel as the CN in the new row corresponding to the label number from step 6, and repeat this step until the fish enters a real channel.
Else, if the fish enters a $\text{CN} < -1000$, which is a temporary channel, then, assign a flag value of -1, repeat step 5, subsequently assign the new channel as the CN in the new row corresponding to the label number from step 6, and repeat this step until the fish enters a real channel.
- Step 8: Assign a random position $\{0 \text{ or } L, y(t_{1-F}), zy(t_{1-F})\}$ in the new channel and move the fish in a time step of Δt_F using the algorithm in Figure 5.

Figure E.3. Tree search algorithm for routing through complex channel junctions.

We provide a concrete example to elucidate steps 5 to 7 in Figure E3 (see Figure E4):
Let a fish be at the upstream end of channel 156 to the left of the critical streakline. Then,

Step 2: The flag value is -1.

Step 5: The CN is -156. -156 appears in the lookup table in row 230:

13002	13002	-156	-155
-------	-------	------	------

The labels of the new channels are 1 for 155 and 2 for 13002.

Step 6: The fish enters CN 13002. The label value is 2.

Step 7: Since the new $\text{CN} > 1000$, the flag value is -1. The new CN is thus -13002.

Step 5: This appears in the lookup table in row 229:

13001	13001	-13002	167
-------	-------	--------	-----

The labels of the new channels are 1 for 167 and 2 for 13001.

Step 6: Since the label value in Step 6 was 2, the new channel is 13001.

The flag value is now -1. The new CN is -13001.

Step 5: This appears in the lookup table row 228:

13000	13000	154	-13001
-------	-------	-----	--------

The labels of the new channels are 1 for 13000 and 2 for 154.

Step 6: Since the label value in Step 6 was 2, the new channel is 154.

Thus, channel 154 is the new channel that the fish enters. We then proceed to step 8 and estimate the new position of the fish.

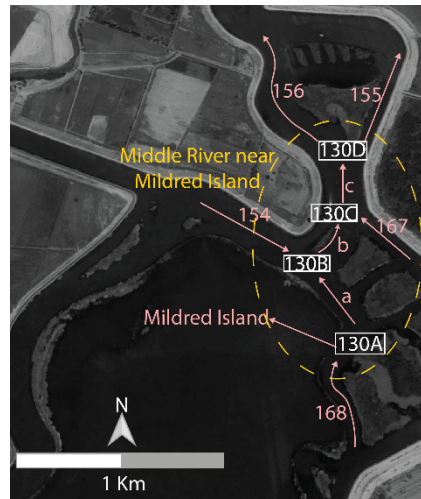


Figure E4. Schematic of junction 130. The alphabets A-D correspond to sub-junctions numbered 130, 13000, 13001, 13002 respectively, and the alphabets a-d correspond to channels numbered 13001, 13002, and 13003, respectively in the lookup table.

Appendix F: Toy PTM for initial analysis and screening

A simplified random walk model was implemented in the R programming language by Russ Perry (p.c.) to screen model parameter interactions and determine the parameter value bounds for optimizing some model parameters. This was implemented as a three-reach, one-junction coarse and highly simplified representation of the Delta (Figure F.1). The *toy PTM* simulates fish movement, routing, and survival through the three reaches. An additional reach was included within each route solely for the purposes of providing two detection stations within each route, which was required for separately estimating survival in reaches 2 and 3 from acoustic telemetry detection data. For this last reach, survival is set to one and no particles are simulated. The movement of fish from reach one into reach 2 or 3 is by random chance based on routing probabilities, Ψ for reach 2 and $1 - \Psi$ for reach 3 which are equal to the ratio of flow through the reach and the flow in reach 1. The X-T model formulation similar to Equation A10 in Appendix A was adopted to model survival through the reaches. The behavior model in the *toy PTM* is identical to that in *ePTM v2*. All behavioral and mortality parameters are reach-specific.

The *toy PTM* runs a random walk of particles using water velocities from the Sacramento River from October 2018 to March 2019. Reach 1 uses water velocities from the Sacramento River at Freeport, Reach 2 uses velocities from Sacramento River below Georgiana Slough, and Reach 3 uses velocities from the Sacramento River at Rio Vista.

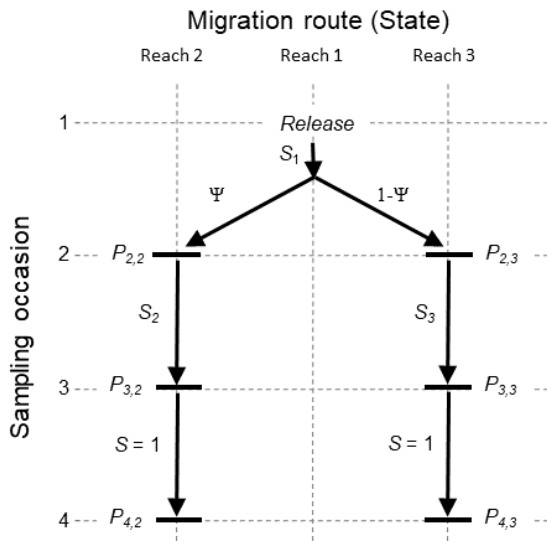


Figure F.1. Schematic of channel structure and associated mark-recapture model parameters.

The *toy PTM* was run multiple times with 500 fish each time with different parameter value combinations to study the effects of interactions between model parameters, as well as to determine the ranges of the λ and ω parameters that recovered survival rates obtained from the analysis of Perry et al. (2018).

Appendix G: Evaluation of space-filling algorithms for initial parameter selection

To select the optimal space-filling algorithm, we compared ten space-filling algorithms using the R package DiceEval (Dupuy et al. 2015) including random selection, Latin hypercube sampling, maximin Latin hypercube sampling, Halton filter, Sobol filter, Sobol-Owen filter, Sobol-Faure-Tesuka filter, Sobol-Owen-Faure-Tesuka filter, maximum separation criterion, the WSP and Strauss methods. We performed an initial screening of the approaches with 20 2D points and compared two measures of volume occupancy: (i) the Greenwood statistic, which measures how clumped points are when projected onto a line slicing the 2D plane at various angles, and (ii) the distribution of points along the direction in which the points are most clumped together. Based on this initial assessment, we selected the random selection, maximin Latin hypercube sampling, maximum separation criterion, WSP method and Strauss methods as promising candidates for a full evaluation with the 5,000 design points.

To select between the remaining candidates, we used four measures of volume occupancy: the mesh ratio, which measures the closeness of the designated points to a uniform n-dimensional mesh, the minimum multidimensional Euclidean separation between points which goes from 0 to 1, the coverage which measures the deviation of minimum multidimensional separation between points to the mean separation between points, and the clumpiness of points in all possible two-dimensional projections of the multidimensional points. Using the maximum separation method with a minimum separation criterion of 0.244 produced the best performance of all the approaches across the four metrics (Figure G1).

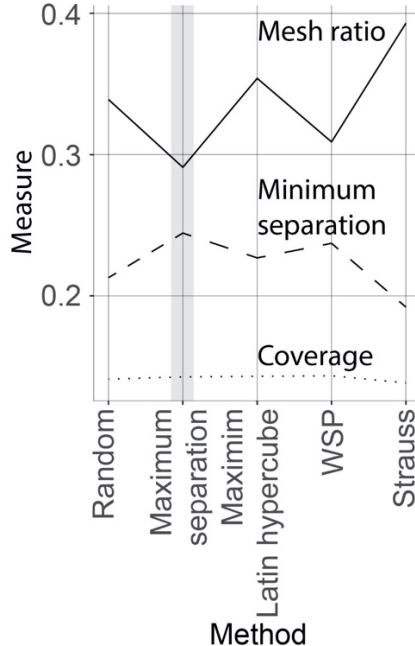


Figure G1. Selection criteria for candidate space-filling approaches. The values of mesh ratio (higher is better), minimum separation (higher is better) and coverage (lower is better). All selected candidate algorithms produced 11-dimensional points with satisfactory clumpiness. The maximum separation criterion was selected (shaded box) based on its overall performance across the four volume occupancy measures.

Appendix H: Log-likelihood goodness-of-fit measure for travel time distributions

In Section 3.3, we outlined the model calibration process, in which one of the goodness-of-fit measures was a log-likelihood of travel time distributions. Here, we show how this is estimated. There are X releases in Y reaches, with N_{ij} fish released in the i^{th} release in the j^{th} reach. Of the released fish, the number that arrive at the downstream end of the reach are N'_{ij} . These arrive at ordered times $\mathcal{T}_{ij} = \{t_{ij,1}, t_{ij,2}, \dots, t_{ij,k}, \dots, t_{ij,N'_{ij}}\}$. Also, the survival estimated from the data in each release and for each reach is S_{ij} .

Travel time distribution

For release i and reach j , and for a given design ePTM parameter set $\theta_{s \in [1, 5000]} = \{\mu_{\text{Swim}}, \sigma_{\text{Swim}}, p_{\text{DaySwim}}, p_{\text{Persistence}}, p_0, b, c, p_{\text{STST}}, u_{\text{STST}}, \lambda, \omega\}_s$ there are M replicates for each of the N_{ij} fish. For the k^{th} fish, let there be M'_k replicate simulated arrivals at ordered times $\tau_{ijk,1}, \tau_{ijk,2}, \dots, \tau_{ijk,M'_k}$. From this set of ordered times, we produce an arrival time distribution $f_{ijk}(t)$ for the k^{th} fish over all the M replicate runs.

Then, the probability of the travel time of the k^{th} simulated fish being $t_{ij,k}$ is

$$P(t_{ij,k} | \theta_s) = f_{ijk}(t = t_{ij,k} | \theta_s) \cdot d\tau$$

Then, the likelihood of the observed travel time distribution for reach i and release j is

$$L_{ij} \left(t_{ij,1}, t_{ij,2}, \dots, t_{ij,N'_{ij}} \middle| \theta_s \right) = \prod_{k=1}^{N'_{ij}} P(t_{ij,k} | \theta_s) = d\tau^{N'_{ij}} \prod_{k=1}^{N'_{ij}} f_{ijk}(t = t_{ij,k} | \theta_s)$$

so that the log-likelihood is

$$\log L_{ij} \left(t_{ij,1}, t_{ij,2}, \dots, t_{ij,N'_{ij}} \mid \theta_s \right) = N'_{ij} \log d\tau + \sum_{k=1}^{N'_{ij}} \log f_{ijk}(t = t_{ij,k} \mid \theta_s) \quad \dots (H1)$$

If the k^{th} simulated fish always dies in all of the replicates, then

Now, the log-likelihood across all releases within a given reach for θ_s is

$$\log L_j \left(\cup_{i=1,j=1}^X \mathcal{T}_{ij} \mid \theta_s \right) = (\sum_{i=1}^X N'_{ij}) \log d\tau + \sum_{i=1}^X \sum_{k=1}^{N'_{ij}} \log f_{ijk}(t = t_{ij,k} \mid \theta_s) \quad \dots (H2)$$

Let the set $\theta_j^{\text{Optimal}}$ be the set of values of θ_s that maximizes $\log L_j \left(\cup_{i=1,j=1}^X \mathcal{T}_{ij} \mid \theta_s \right)$.

Now, the overall log-likelihood of the data is to be maximized given different parameter combinations in the various reaches and releases is

$$\log L \left(\cup_{i=1,j=1}^{X,Y} \mathcal{T}_{ij} \mid \theta_j \right) = \sum_{j=1}^Y \log L_j \left(\cup_{i=1,j=1}^X \mathcal{T}_{ij} \mid \theta_j \right) \quad \dots (H3)$$

Clearly, the $\theta_j^{\text{Optimal}}$'s will also maximize the overall log-likelihood of the data.

Steps in the process

1. Perform ePTM simulations with M replicates for each fish in each reach and release for 5,000 design ePTM parameter sets.
2. Get the distributions of travel time of the k^{th} fish, $f_{ijk}(t)$, from the replicate ePTM results.
3. Compute $\log L_{ij} \left(t_{ij,1}, t_{ij,2}, \dots, t_{ij,N'_{ij}} \mid \theta_s \right)$ for the given reach, release and design parameter sets, and sum these up across releases for a given reach and for a given design parameter set s to get $\log L \left(\cup_{i=1,j=1}^X \mathcal{T}_{ij} \mid \theta_s \right)$.
4. Find $\max [\log L \left(\cup_{i=1,j=1}^X \mathcal{T}_{ij} \mid \theta_s \right)]$, and get ϕ_j^{Optimal} corresponding to this value.
5. The set $\cup_{j=1}^Y \phi_j^{\text{Optimal}}$ will be the optimal parameter combination over the entire domain.

Appendix I: Conversion of survivals reported at Benicia to survivals at Chipps Island

In order to compare the model results to the CJS-estimated survivals from the data in situations where the survival at Benicia was reported, we adopted the following approach.

Let the distance between Benicia and Chipps Island be $l = 19.4\text{Km}$. Let the distance between the nearest upstream station to Benicia (upstream of Chipps Island as well) used in the CJS analysis be x . Then the distance between this station and Chipps Island is $x - l$. Let the cumulative survival reported at Delta entry be S_E . Let the cumulative survival reported at Benicia be S_B . We need the survival rate between Delta entry and Chipps Island, S_{E-C} .

As survival compounds over distance, the S_B can be written in terms of the cumulative survival at the nearest station upstream of Benicia in the CJS analysis as

$$S_B = S_X \cdot S_{X-B} \Rightarrow S_{X-B} = \frac{S_B}{S_X} \quad \dots (I1)$$

where S_{X-B} is the survival rate between the upstream station and Benicia. By the same token, given a spatially uniform survival rate per unit distance between the upstream station and Benicia, s , we must have

$$S_{X-B} = s^x \Rightarrow s = S_{X-B}^{1/x} \quad \dots (I2)$$

and the survival rate between this upstream station and Chipps Island must be

$$S_{X-C} = s^{x-l} = S_{X-B}^{(x-l)/x} = \left(\frac{S_B}{S_X} \right)^{(x-l)/x} \quad \dots (I3)$$

We must also have, by the principle of cumulative survival, the cumulative survival to Chipps Island as

$$S_C = S_X \cdot S_{X-C} = S_X \cdot \left(\frac{S_B}{S_X}\right)^{(x-l)/x} \quad \dots \text{ (I4)}$$

But, it must also be true that

$$S_C = S_E \cdot S_{E-C} \quad \dots \text{ (I5)}$$

Then, by substituting Equation (I4) into Equation (I5), we get

$$S_{E-C} = \frac{S_C}{S_E} = \left(\frac{S_X}{S_E}\right) \cdot \left(\frac{S_B}{S_X}\right)^{(x-l)/x} \quad \dots \text{ (I6)}$$

We used Equation (I6) to compute the survival rate between Delta entry and Chipps Island in those cases when the CJS survival was reported at Benicia. In one instance (Coleman hatchery Fall-run in 2013), when zero mortality was reported at Benicia, we instead applied the same approach but with survival reported at GoldenGateE instead of Benicia.